AIMS Mathematics, 9(4): 9059−9090.
DOI: 10.3934/math.2024441
Received: 19 December 2023
Revised: 04 February 2024
Accepted: 23 February 2024
Published: 05 March 2024

http://www.aimspress.com/journal/Math

Research article

Utilization of the Crank-Nicolson technique to investigate thermal enhancement in 3D convective Walter-B fluid by inserting tiny nanoparticles on a circular cylinder

Fu Zhang Wang[1], Muhammad Sohail[2,*], Umar Nazir[3], Emad Mahrous Awwad[4] and Mohamed Sharaf[5]

[1] Department of Mathematics, Nanchang Normal College of Applied Technology, Nanchang 330108, Jiangxi, China
[2] Institute of Mathematics, Khwaja Fareed University of Engineering & Information Technology, Rahim Yar Khan 64200, Pakistan
[3] Department of Mathematics, Faculty of Science, Khon Kaen University, Khon Kaen 40002, Thailand
[4] Department of Electrical Engineering, College of Engineering, King Saud University, P.O. Box 800, Riyadh 11421, Saudi Arabia
[5] Department of Industrial Engineering, College of Engineering, King Saud University, P.O. Box 800, Riyadh 11421, Saudi Arabia

* **Correspondence:** Email: muhammad_sohail111@yahoo.com.

Abstract: The current study is based on the mechanism of mixed convection and solar thermal radiation in Walters'-B fluid considering tera-hybrid nano-structures using convective boundary constraints (CBC) and (CHF) constant heat flux. The heat transmission phenomenon of the current study is taken into account under the influence of triple-suspended nanoparticles. The current problem has several potential applications, including improvements in solar thermal energy systems, nanofluids, aerospace, cooling processes, automotive engineering, and numerical modeling methods. A numerical approach, namely Crank-Nicolson, is utilized in the modeling of 3D Walter's B fluid past over a 3D circular cylinder whose radius varies sinusoidally for evaluation of velocity and temperature distributions. For mathematical modeling, the Cartesian coordinate system was used for the current study. Comparative analysis between constant heat flux (CHF) and convective boundary constraints (CBC) was demonstrated graphically against multifarious parameters towards the temperature profile and velocity profiles along the x-axis and in the y-axis. Moreover, comparative analysis for dissimilar

parameters was manifested for Nusselt number through tables, and graphically for skin friction coefficient and Nusselt number and has shown excellent accuracy. It was estimated that by enhancing values of Q_{sr}, C, H_s and Ec, it was addressed that temperature curve increases for CHF and CBC cases.

Keywords: heat transfer; tetra-hybrid nanofluid; Walters'-B fluid; solar thermal radiation; circular cylinder; non-Fourier's law; finite element procedure; Maple software
Mathematics Subject Classification: 80A05, 80A19, 65M06

Nomenclature

Y, X, Z	Space coordinates *(m)*	u, w, v	Velocity components (ms^{-1})
A, B	Constant (-)	ν	Kinematic viscosity (m^2s^{-1})
K_0	Fluid number (-)	ρ	Density (Kgm^{-3})
B_0	Magnetic number $(NA^{-1}m^{-1})$	E	Eclectic field number (-)
σ	Electrical density (Sm^{-1})	K	Thermal conductivity (Wm^{-1})
$\bar{T}$	Temperature (K)	Q_0	Heat source (-)
A_{sr}	Solar number (-)	T_∞	Ambient temperature (K)
λ	Relaxation time (-)	γ	Deborah number (-)
v_e	Free stream velocity (ms^{-1})	u_e	Free stream velocity (ms^{-1})
Θ	Dimensionless temperature (-)	T_w	Wall temperature (K)
We	Weissenebrg number (-)	M	Magnetic number (-)
Pr	Prandtl number (-)	Q_{sr}	Solar thermal radiation number (-)
β	Time relaxation number (-)	H_s	Heat source number (-)
$\omega_4, \omega_3, \omega_2, \omega_1$	Volume fractions of nanoparticles (-)	C_f, C_g	Skin friction coefficients (-)
Nu	Nusselt number (-)	Re	Reynolds number (-)
Tetra	Tetra-hybrid nanofluid (-)	EMHD	Electric magnetic hydro-dynamic (-)
Tri	Tri-hybrid nanofluid (-)	hyb	Hybrid nano-fluid (-)
$3D$	Three-dimensional (-)	x_e	streamline flow number (m)
β^*	Constant (-)	C	Nodal stagnation number (-)
$\boldsymbol{\tau}$	Vector tensor (FA^{-1})	P	Pressure (Pa)
I	Identity matrix (-)	μ	Viscosity $(Kgm^{-1}s^{-1})$
δ	Thermal slip parameter (-)	k_1, k_0	Fluidic numbers (-)
div	Divergence (-)	∞	Infinity (-)
q_w	Heat wall flux (Wm^{-2})	Al_2O_3	Aluminum oxide (-)
Fe_3O_4	Iron oxide (-)	Cu	Copper (-)
TiO_2	Titanium oxide (-)	Q_w	Wall flux (Wm^{-2})
τ_w	Wall shear stress (Pascal)	$\Delta\eta$	Indicate space point (-)
i	Mesh points (-)	η	Independent variable (-)
$\boldsymbol{A_1}, \boldsymbol{A_2}$	Shear rates (-)	S, T	Dimensionless velocities (-)
Θ	Dimensionless temperature (-)	F_i, G_i and Θ_i	Dimensionless velocity and temperature profiles (-)

1. Introduction

Several investigations have been conducted for non-Newtonian models due to their wider applications. A key component of producing energy is heating transfer such as geothermal energy extraction, solar energy collection, and combustion in power plants. Heat transfer principles are used to control thermal conditions in radiator design, car climate control systems, materials for buildings, solar water heaters, natural gas liquefaction, energy production, nuclear plants, food preservation, generating steam, hyperthermia treatments, and engine cooling systems. Shafiq et al. [1] assessed the third-grade fluid influenced by thermal radiation in the extended cylinder. Chemically reactive Walter's B fluid towards the asymmetric channel was analyzed by Vadiya et al. [2]. With the implementation of sensitive analysis, Walter's B Nano fluidic stagnant point flow due to Riga surface was controlled by Shafiq et al. [3]. In this study, the Buongiorno model was utilized. Heat as well as mass transmission within the free convection flow demeanor of Walter's B fluid under the effect of magnetic field was examined by Khan et al. [4]. Hayat et al.'s [5] investigation was based on Walter's B fluid bounded by an extending surface under the influence of Newtonian heating. Madallal et al.'s [6] work was based on the analytical investigation of combined mass as well as heat transmission with magnetized flow towards a vertically oscillating plate established in the penetrating medium. Heat source/sink together with viscous dissipation effects for the magnetized chemically reactive Walter's B fluid in a curved shape convectively heated channel was studied by Tanveer et al. [7]. Radial effects within the mixed convection towards the Walter's B Nano fluidic flow demeanor in a circular shaped cylinder in convective together with constant heat flux was investigated by Mahat et al. [8]. The thermal stratification phenomenon was considered by Shah et al. [9] for the thermography pertains to ferromagnetic Walter's B fluid. Johnson and Olajuwon [10] analytically studied the radial with production/absorption and thermo diffusion effects along with chemical reactions and thermal diffusion in the Walter's B fluid, which was subjected to a penetrating medium. The prime intention of Asifa et al.'s [11] study relies on the investigation of combined time-controlled (ramped) limiting conditions towards the electro-osmotic flow behavior of chemically reactive and radiative Walter's B fluid. Bio-convective Walter's B Nano fluid was considered by Shafiq et al. [12] and studied the thermophoresis along with Brownian movement in a cylindrical shape disk influenced by artificial neural networks (ANN). A numerical approach based on a radial stagnant point flow demeanor of magnetized Walter's B Nano fluid was given by Khan and Alzahrani [13], who investigated the Joule heating together with activation energy and chemical reaction impacts. Thermally radiative magneto Walter's B flow demeanor passing over a semi-infinite vertical-shaped plate under the heat source along with viscous dissipation influence was analyzed by Damala et al. [14]. 2-D magnetized Walter's liquid B occurrence consisting of copper nanoparticles bounded by an extending sheet subjected to a penetrating medium was discussed by Vanitha et al. [15]. In this study, thermal radiation effects with mass transpiration were considered. A numerical approach based on the investigation of bio-convective transmission of magnetized Walter's B Nano fluid through a cylindrical disk under the Brownian movement and thermophoresis impacts was given by Waqas et al. [16]. Moreover, thermal radiation, motile organisms, and varying thermal conductivity effects were also considered in this analysis. Peristaltic transmission of an electro-magnetized Walter-B fluid under the influence of heat source and thermal radiation along slip condition was discussed by Makinde et al. [17]. An electro-magnetized laminar flow demeanor was examined by M. V. Krishna [18] based on elastic-viscous (Walter's B) in a circular shaped cylinder under the impacts of Hall and ion slip. Magnetized unsteady viscoelastic conducting Walter's B liquid amongst the binary penetrating concentric circular shaped cylinder was discussed by Kumar and Pant [19]. Moreover, Huang and Feng's [20] analysis is based on the 2-D steady flow demeanor of viscoelastic

fluid under the wall effects subjected to a circular cylinder. Moatimid and Zekry [21] proposed the non-linear stability analysis pertaining to electro-iscoelastic Walter's B fluid subjected to penetrating media. Karim et al. [22] studied the heat production impacts towards the free convected boundary layer flow demeanor bounded by a horizontally shaped circular cylinder having constant surface heat flux. Combined effects of heat transmission with chemical reactions for the blood flow pertaining to Walter's B fluid in a tapered artery were analyzed by Nadeem and Akbar [23]. Steady flow demeanor referring to power-law fluids over a circular shape cylinder was examined by Bharti et al. [24]. Entropy production analysis for the Walter's B Nano fluidic flow under the impacts of swimming gyro tactic microorganisms was reported by Naz et al. [25]. A mathematical model was proposed by Khan et al. [26] based on the MHD flow demeanor of Viscous fluid bounded by a non-linear extending surface under the influence of Joule heating and viscous dissipation with velocity and thermal slip condition. Thermophoretic particle deposition impacts under the combined pressure and buoyancy forces occurrence of magnetized Walter's B Nano fluid through an extending surface was examined by Chu et al. [27]. Alzahrani and Khan's [28] work was based on the heat conduction significance in dual reactive flow behavior of Walter's B fluid under the impacts of activation energy and radiative flux. An analytical approach was presented by Ragaran et al. [29] on entropy production towards Walter's liquid B fluid past over an extending sheet under elastic deformation. KASIM [30] analyzed the mixed as well as free convective boundary layer flow demeanor based on viscoelastic fluid subjected to a horizontal circular shape cylinder. Ahmad et al. [31] examined the non-axisymmetric Homann stagnant occurrence referring to unsteady Walter's B Nano fluid through a vertical-shaped cylindrical disk. Hayat et al. [32] analyzed the third-order flow demeanor of an incompressible fluid bounded by a circular-shaped cylindrical tube. Akinbo [33] examined the heat and mass transportation of a Walter's B fluid under the impact of thermal diffusion with convective limiting conditions bounded by a vertically extending surface. Analysis based on heat transmission was discussed by Khan et al. [34] for the unsteady free convection occurrence of Walte's B fluid. A numerical approach based on mixed convection Walter's B Nano fluidic flow demeanor through extending surface under the influence of Newtonian heating and mass transmission was proposed by Qaiser et al. [35]. Gangadhar et al. [36] investigated the convective thermal transmission properties of a hybrid nano-liquid combination containing magnesium oxide (MgO) and gold (Au) tiny particles. They examined slip properties on nodal/saddle stagnation point border layer movement with sticky dissipation impact. Gangadhar et al. [37] explored the impressions of Lorentz power and convective warming boundary on second-grade tiny liquid movement beside a Riga configuration. They found that the delivery of the deliberation of nanoelements rises with the rise of the thermophoretic feature. Gangadhar et al. [38] addressed the structures of mass and thermal transference sensations of two-dimensional viscid liquid movement of Oldroyd-B nano liquid on a vertical extendible piece. They measured the diverse convection and tending magnetic pitch impressions that hold gyrotactic microbes. Kotha et al. [39] analyzed the two-dimensional magnetohydrodynamic movement and mass and thermal transportation spectacles of liquid-based tiny-fluid including gyrotactic microbes over a vertical platter using thermal absorption or generation. They discovered that slog pressure rate and motile microbe sketches are augmented through the development of a magnetic field. Gangadhar et al. [40] inspected the viscoelastic Oldroyd-B tiny fluid movement passed a vertically extending pane with spinning gyrotactic microbes. Gangadhar and Chamkha [41] studied the entropy creation for the fascinated joined stress of liquid passing a leaky extending cylinder, which generates convective heat transport. They inspected entropy creation sponsors the progression of the magnetic arena and the Brinkman quantity. Gangadhar et al. [42] added solar radiation and convective warming portents to the temperature equation to grow the thermal circulation spectacles. They applied zero mass fluctuation sensations at the border. Gangadhar et al. [43]

established the hydrothermal distinction for two hybrid tiny liquids, and an acquainted tiny fluid movement over an extendible spinning cylinder. They discovered that both velocities are condensed for the magnetic fluctuation. Gangadhar et al. [44] scrutinized movement and volumetric entropy formation and convective warmth transference on Powell-Eyring hybrid tiny liquid. They explored hybrid tiny liquids that join the space over the efficient horizontal absorbent elongating surface. Gangadhar et al. [45] premeditated the corporal structures of the bioconvective MHD stream of a pair stress liquid over an upper horizontal shallow with radiation and viscid dissipation imitations. They investigated expanding standards of pair stress and magnetic factor weakening the velocity. Gangadhar et al. [46] surveyed the apparatus of radiative Walter's B tiny liquid on a revolving cone under magnetic command. The Brownian indication factor is found to have contradictory impacts on heat and mass transport proportions, accompanied by thermal and concentration arenas. Bhargavi et al. [47] discovered the hydrothermal presentation of a hybrid tiny-liquid made of graphene, and gold/polydimethylsiloxane among two cuddling sheets. They found that the Deborah quantity defined stress relaxation spectacle causes the movement arena and thermal warmth transference to be less effective when liquids are stirring.

Thermal efficiency with the entropy approach was evaluated by Hanif et al. [48] towards the magneto-hybrid Nano liquid in accordance with variable viscosity. In this evaluation, the Crank-Nicoloson approach was used. Similarly, Hanif et al. [49] also considered the numerical approach namely, Crank Nicoloson, for the conventional water-reliant hybrid (aluminum alloy) Nanofluidic occurrence bounded by expandable horizontal plate exposed to thermal resistive impact. Homotopic simulation was conducted by Shamshuddin et al. [50] for the magnetized bio-convected flow demeanor of water-reliant hybrid Nano liquid past over a thermally convected exponential expanding surface. 3-D bio convected occurrence pertaining to Casson Nano liquid influenced by non-linear thermal radiation bounded by spinning frame and slip effect was investigated by Li et al. [51]. In this investigation, Homotopy approach was utilized. Imran ullah et al. [52] scrutinized the 3-D bio-convected occurrence referring to Casson Nano liquid subjected to the convectively heated extendable surface under consideration of thermal production (absorption) impacts. Thermal features, occurrence, and contrast among the suspended Nano-size particles, namely copper (Cu) and silver (Ag), in sodium alginate within the Sutterby Nano liquids in solar storage were discussed by Bouslimi et al. [53]. A bio-full application based on thermal efficiency and convected analysis owing to the chemically reactive flow demeanor of viscoelastic Nano-size material under consideration of advanced heat theories was presented by Aldabesh and Tili [54]. A molecular dynamics analysis for the elimination of heavy metals from wastewater with the help of Polymers in the industry was studied by Le et al. [55]. Sajjad et al. [56] focused on the performance investigation of fin-prolonged thermal exchangers exposed to distinct Nano fluidic applications. Hussain et al. [57] utilized the Rathakrishnan Kundu-Lakshmanan equation and analyzed the bifurcation and also Chaos across the traveling wave solution within the Optical fibers. Bhatti et al. [58] covered the electrically magnetized combustible convective transportation within a vertical duct. This study was based on the Carreau fluid model. Moreover, Lie group analysis with a robust computational technique was considered by Bhatti et al. [59] to investigate the mass transmission phenomena across the Jeffery fluid model. A thermal investigation based on radiative ternary hybrid Nano liquid exposed to thermal radiation configured by a convectively heated sinusoidal shape cylinder was conducted by Simda et al. [60]. The objective of Tlili et al.'s [61] work is based on the Nano fluidic flow demeanor with the dispersion of non-Newtonian material exposed to the additional effect of an external heating source bounded by a bilateral oscillatory regime. A molecular dynamic study based on Perovskite materials and the usage of biomaterials in the solar cell application was presented by Le and Tlili [62]. Graphene oxide (GO), owing to its unique properties

such as pH responsiveness, emerged as significant nanocarrier. Le et al. [63] explored the absorption and also release demeanor of (DOX) drugs within the GO nanocarriers in comparison to pure Graphene. Elmonem et al. [64] addressed the combined impacts of thermal production (absorption) with activation energy across the magneto water-reliant hybrid Nano liquid $(GO - MoS_2)$ flow demeanor bounded by a spinning disk. The pivotal purpose of the research by Eid et al. [65] is based on energy bandgap and thermal features pertaining to non-Darcian magnetized spinning hybrid Nano liquid thin film occurrence. Ullah et al. [66] studied unsteady Newtonian fluid in the transport mechanism of heat utilizing nanofluid on a circular cylinder. They have incorporated a shooting approach for numerical results. Raizah et al. [67] discussed the features of micropolar fluid incorporating a hybrid nanofluid with motile microorganisms and stagnation point flow on a circular cylinder. Gholinia et al. [68] investigated the motion of a hybrid nano-fluid in Newtonian fluid on a circular cylinder with convective boundary conditions; they used an analytical approach. Dinarvand et al. [69] expressed investigations for a series of solutions of nanofluid in a Newtonian fluid using no-slip conditions on a circular cylinder. They incorporated the HAM approach to investigate numerical consequences. Literature reviews [66−69, 79−83] reveal that there are no investigations based on 3D Walters'-B fluid considering tetra-hybrid nano-fluid on a circular cylinder. The current study contains magnetic field, non-Fourier's law, and solar thermal radiation.

The heat transmission phenomenon in a fluid known as Walters'-B fluid is described. The combined effects of solar thermal radiation and mixed convection are our focus. Within the fluid, tera-hybrid nanostructures are taken into consideration while being influenced by constant heat flux (CHF) and convective boundary constraints (CBC). Our goal is to comprehend how the introduction of tetra-hybrid nanoparticles affects the behavior of the heat transmission process. The current study can be used as a model for an ultra-high cooling system, and because the system has superior thermal diffusivity and thermal conductivity over hybrid nano-fluid and nanofluid, it makes an excellent coolant.

2. Flow and development of the model

The flow model describes the behavior of 3D Walters'-B towards a 3D circular cylinder such as the radius of a circular cylinder differs sinusoidally. Every point related to "O", "N", and "M" have minimum and maximum radii associated with stagnation points. Moreover, the circular cylinder has three components based on w, u and v in Z, X and U. Stream velocities are defined as $u_e(= Ax)$ and $v_e(= Bx)$ where B and A are free stream constants. Here, x_e reveals streamline flow that is defined as $x_e\left(= \beta^* y^{1/C}\right)$ while β^* illustrates the constant associated with a particular streamline. It states that the range of nodal stagnation factor is $0 < C < 1$, while the range associated with $-1 < C < 0$ is revealed by Figures 1 and 2. Walter's-B fluid [70] is known as non-Newtonian fluid. Such kind fluid has several applications that are food industries, cosmetics, suspended liquids, clay coating, paper production, paints and emulsion formation, polymer solutions, cosmetics, food items, and paints. It was noticed that Walter's B liquid is called non-Newtonian fluid [71], while engine oil is found as non-Newtonian fluid [72,73]. The vector of tensor $(\boldsymbol{\tau})$ related to Walter's-B fluid is

$$\boldsymbol{\tau} = -PI + \mu(\boldsymbol{A_1}) - k_0(\boldsymbol{A_2}) + k_1(\boldsymbol{A_1})^2. \tag{1}$$

Here, P, I, μ, k_0 and k_1 are pressure, identity matrix, dynamic viscosity, and fluid parameters. The velocity field and tensor in components form is defined as

$$div\tau_y = \nu_{THb}\frac{\partial^2 u}{\partial Y^2} - \frac{K_0}{\rho_{THb}}\left[\frac{\partial}{\partial X}\left(u\frac{\partial^2 u}{\partial Y^2}\right) + v\frac{\partial^3 u}{\partial Y^3} - \frac{\partial u}{\partial Y}\frac{\partial^2 u}{\partial X \partial Y}\right]. \tag{2}$$

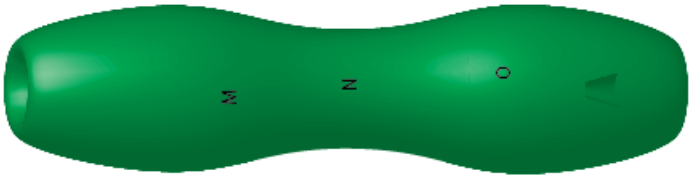

Figure 1. Physical description of the model.

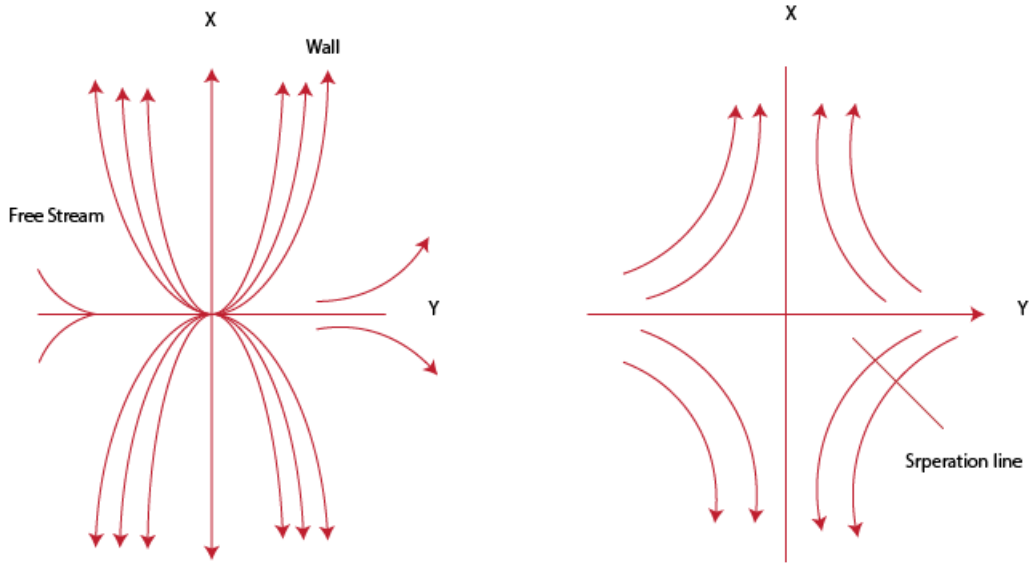

(a) (b)

Figure 2. Nodal attachment point (a) and saddle attachment point (b).

2.1. Assumptions regarding the flow model

The mathematical procedure has been introduced considering the following assumptions:

1) Non-Fourie's law, Walters'-B and EMHD flow;
2) Incompressible and steady flow are considered;
3) Three-dimensional flow is assumed;
4) Heat source and magnetic field are taken out;
5) Convective heat flux and constant heat flux are addressed;
6) 3D-steady and convective boundary constraints;
7) Heat source, magnetic strength and solar thermal radiation;
8) Circular cylinder, boundary layer procedure and engine oil;
9) The flow contains three types of nanofluid.

Using the above assumptions and $div\tau_y$ in governing equations that capture Walters'-B [67−69] and EMHD flow can be modeled as

$$\frac{\partial u}{\partial r}+\frac{\partial w}{\partial Z}+\frac{u}{r}=0, \tag{3}$$

$$u\frac{\partial u}{\partial X}+v\frac{\partial u}{\partial Y}+w\frac{\partial u}{\partial Z}-A^2X=\nu_{Tetra}\frac{\partial^2 u}{\partial Z^2}-\frac{K_0}{\rho_{Tetra}}\left[\frac{\partial}{\partial X}\left(u\frac{\partial^2 u}{\partial Z^2}\right)+v\frac{\partial^3 u}{\partial Z^3}-\frac{\partial u}{\partial Z}\frac{\partial^2 u}{\partial X\partial Z}\right]+\frac{\sigma_{Tetra}}{\rho_{Tetra}}(EB_0-B_0u), \tag{4}$$

$$u\frac{\partial v}{\partial X}+v\frac{\partial v}{\partial Y}+w\frac{\partial v}{\partial Z}-B^2Y=\nu_{Tetra}\frac{\partial^2 v}{\partial Z^2}-\frac{K_0}{\rho_{Tetra}}\left[\frac{\partial}{\partial X}\left(u\frac{\partial^2 u}{\partial Z^2}\right)+v\frac{\partial^3 u}{\partial Z^3}-\frac{\partial u}{\partial Z}\frac{\partial^2 u}{\partial X\partial Z}\right]+\frac{\sigma_{Tetra}}{\rho_{Tetra}}(EB_0-B_0u), \tag{5}$$

$$u\frac{\partial \bar{T}}{\partial X}+v\frac{\partial \bar{T}}{\partial Y}=\frac{k_{Tetra}}{(\rho c_p)_{Tetra}}\frac{\partial^2 \bar{T}}{\partial Z^2}+\frac{Q_0}{(\rho c_p)_{Tetra}}(\bar{T}-T_\infty)+\frac{A_{sr}Q_0}{(\rho c_p)_{Tetra}}EXP(-A_{sr}Z)-\lambda\begin{bmatrix}\left(w\frac{\partial}{\partial Z}+u\frac{\partial}{\partial X}\right)u\bar{T}_X+\left(w\frac{\partial}{\partial Z}+u\frac{\partial}{\partial X}\right)w\bar{T}_Z+2uw\bar{T}_{XZ}\\ u^2\bar{T}_{XX}+w^2\bar{T}_{ZZ}-\frac{Q_0}{(\rho c_p)_{Tetra}}\left(w\frac{\partial}{\partial Z}+u\frac{\partial}{\partial X}\right)\bar{T}\end{bmatrix}. \tag{6}$$

Along with boundary constraints [67−69]

$$\left.\begin{matrix}v=0,w=0,\bar{T}-T_w=\gamma K_{Tetra}\frac{\partial \bar{T}}{\partial Z}:Z=0\\ v\to v_e,u\to u_e,\bar{T}\to T_\infty \text{ at } Z\to\infty\end{matrix}\right\}. \tag{7}$$

And

$$\left.\begin{matrix}v=0,w=0,\bar{T}=-\frac{q_w}{k_{Tetra}}:Z=0\\ v\to v_e,u\to u_e,\bar{T}\to T_\infty \text{ at } Z\to\infty\end{matrix}\right\}. \tag{8}$$

Similarity quantities [67−69] are defined as

$$u=AXS',v=BYT',w=-\left(A\nu_f\right)^{\frac{1}{2}}(CS+T),\eta=Z\left(\frac{\nu_f}{A}\right)^{\frac{1}{2}},\Theta=\frac{\bar{T}-T_\infty}{T_w-T_\infty}. \tag{9}$$

Using Eq (6) into Eqs (1)−(4), flowing reduced form is

$$S'''-(S')^2\frac{\nu_f}{\nu_{Tetra}}+\frac{\nu_f}{\nu_{Tetra}}TS''-\frac{We\left[2S'S'''-SS^{iv}-(S'')^2\right]}{(1-\omega_1)^{2.5}(1-\omega_3)^{2.5}(1-\omega_4)^{2.5}(1-\omega_2)^{2.5}}+\frac{\nu_f}{\nu_{Tetra}}CTS''+\frac{\sigma_f}{\sigma_{Tetra}}M(E-S')+\frac{\nu_f}{\nu_{Tetra}}=0, \tag{10}$$

$$T'''+\frac{\nu_f}{\nu_{Tetra}}ST''-\frac{We\left[2T'T'''-TT^{iv}-(T'')^2\right]}{(1-\omega_1)^{2.5}(1-\omega_3)^{2.5}(1-\omega_4)^{2.5}(1-\omega_2)^{2.5}}+\frac{\nu_f}{\nu_{Tetra}}CSS''-\frac{\nu_f}{\nu_{Tetra}}C(S')^2+\frac{\sigma_f}{\sigma_{Tetra}}M(E-S')+\frac{\nu_f}{\nu_{Tetra}}C=0, \tag{11}$$

$$\Theta''+\frac{k_{Tetra}\left(\rho c_p\right)_f}{k_f\left(\rho c_p\right)_{Tetra}}S\Theta'+\frac{k_{Tetra}\left(\rho c_p\right)_f}{k_f\left(\rho c_p\right)_{Tetra}}CT\Theta'+\frac{k_f}{k_{Tetra}}H_sPr\Theta+\frac{k_f}{k_{Tetra}}\frac{Pr\lambda Q_{sr}}{k_r}EXP(-\lambda\eta)+\frac{k_{Tetra}(\rho c_p)_f}{k_f(\rho c_p)_{Tetra}}Pr\beta[(S+T)(S'+T')\Theta'+(S+T)^2\Theta''-H_sPr(S\Theta'+T\Theta')]=0. \tag{12}$$

Expressions regarding dimensionless boundary constraints are described below

$$\Theta(0) = \delta \frac{k_{Tetra}}{k_f} \Theta'(0) + 1, \Theta(\infty) = 0,$$

$$T'(\infty) = 1, S(0) = 0, S'(0) = 0, S'(\infty) = 1, T(0) = 0, T'(0) = 0, \tag{13}$$

and

$$\Theta'(0) = -1, \Theta(\infty) = 0, T(0) = 0,$$

$$T'(\infty) = 1, S(0) = 0, S'(0) = 0, S'(\infty) = 1, T'(0) = 0. \tag{14}$$

2.2. Variables of Thermodynamics physical related to tetra-hybrid nano-structures

Correlations associated with tetra-hybrid nano-structures [74] are defined as follows and shown in Table 1.

$$\mu_{Tetra} = \mu_f [(1 - \omega_4)^{2.5} (1 - \omega_3)^{2.5} (1 - \omega_2)^{2.5} (1 - \omega_1)^{2.5}]^{-1}, \tag{15}$$

$$\rho_{Tetra} = \left[(1 - \omega_4) \left\{ (1 - \omega_3)(1 - \omega_2) \left(\left((1 - \omega_1) + \frac{\omega_1 \rho_{s1}}{\rho_f} \right) \right) + \frac{\omega_2 \rho_{s2}}{\rho_f} + \frac{\omega_3 \rho_{s2}}{\rho_f} + \frac{\omega_4 \rho_{s2}}{\rho_f} \right\} \right], \tag{16}$$

$$\frac{k_{Tetra}}{k_f} = \frac{(k_{s4} + 2k_{tri} - 2\omega_4 (k_{tri} - k_{s4}))}{(k_{s4} + 2k_{tri} + \omega_4 (k_{tri} - k_{s4}))}, \frac{k_{Tri}}{k_f} = \frac{\left(k_{s3} + 2k_{hy} - 2\omega_3 \left(k_{hy} - k_{s3}\right)\right)}{\left(k_{s3} + 2k_{hy} + \omega_3 \left(k_{hy} - k_{s3}\right)\right)}. \tag{17}$$

Table 1. Thermal properties of σ, k, ρ and EO (engine oil) [75,76].

	K	ρ	σ
Al_2O_3	32.9	6310	5.96×10^7
Fe_3O_4	80	5180	0.112×10^6
Cu	401	8933	59.5×10^6
EO (engine oil)	0.144	884	0.125×10^{-11}
TiO_2	8.9538	686.2	4250

2.3. Engineering quantities

Branches related to engineering interests are associated with two parameters based on the Nusselt number and skin friction coefficient. Skin friction coefficient (C_f) [67−69] is

$$C_f = \frac{\tau_w}{\rho_{Tetra} (u_w)^2}, \tau_w = \left[\mu_{Tetra} \frac{\partial u}{\partial Z} - K_0 \left(u \frac{\partial^2 u}{\partial X \partial Z} + v \frac{\partial^2 u}{\partial Z^2} + 2 \frac{\partial u}{\partial X} \frac{\partial u}{\partial Z} \right)^3 \right],$$

$$-Re^{\frac{1}{2}} C_f = \frac{(1 - 3We) S''(0)}{(1 - \omega_2)^{2.5} (1 - \omega_1)^{2.5} (1 - \omega_3)^{2.5} (1 - \omega_4)^{2.5}}. \tag{23}$$

Skin friction coefficient (C_g) [67−69] is

$$C_g = \frac{\tau_w}{\rho_{Tetra} (u_w)^2}, \tau_w = \left[\mu_{Tetra} \frac{\partial v}{\partial Z} - K_0 \left(u \frac{\partial^2 v}{\partial X \partial Z} + v \frac{\partial^2 v}{\partial Z^2} + 2 \frac{\partial v}{\partial X} \frac{\partial v}{\partial Z} \right)^3 \right], \tag{24}$$

$$-Re^{\frac{1}{2}}C_g = \frac{(1-3We)T''(0)}{(1-\omega_2)^{2.5}(1-\omega_1)^{2.5}(1-\omega_3)^{2.5}(1-\omega_4)^{2.5}}. \tag{25}$$

The Nusselt parameter [67−69] is addressed as

$$Nu = \frac{xQ_w}{K_{Tetra}(T_\infty - \bar{T})}, Re^{\frac{-1}{2}}Nu = -\frac{k_f}{k_{Tetra}}\Theta'(0). \tag{26}$$

3. Methodology

Maple 18 is utilized for designing the code of the Crank-Nicolson method [77,78]. Several authors have used the mentioned finite difference-based scheme to investigate the numerical solution of various nonlinear problems. In this section, the numerical work of the current model Eqs (7)−(9) is simulated using the Crank-Nicolson scheme which is the numerical approach. The flow chart of the Crank-Nicolson method is illustrated in Figure 1c. It is a famous accurate methodology that is based on a finite difference approach. In the first step, the problem domain is divided into a grid of lines to obtain finite difference equations of Eqs (10)−(14). Steps related to the Crank-Nicolson technique are mentioned below.

The region of the flow is divided into a mesh of finite lines to obtain the solution of the nonlinear system. The finite difference regarding the first order is defined as

$$S_1 = \frac{\partial S}{\partial \eta} = \frac{S_{i+1}-S_i}{\Delta\eta}, T_1 = \frac{\partial T}{\partial \eta} = \frac{T_{i+1}-T_i}{\Delta\eta}, \frac{\partial \Theta}{\partial \eta} = \frac{\Theta_{i+1}-\Theta_i}{\Delta\eta} = \Theta_1. \tag{27}$$

The finite difference regarding the second order is given as

$$\Theta_2 = \frac{\partial^2 \Theta}{\partial \eta^2} = \frac{1}{2}\left[\frac{\theta_{i-1}-2\theta_i+\theta_{i+1}}{(\Delta\eta)^2} + \frac{\theta_{i-1}-2\theta_i+\theta_{i+1}}{(\Delta\eta)^2}\right], \tag{28}$$

$$S_2 = \frac{\partial^2 S}{\partial \eta^2} = \frac{1}{2}\left[\frac{S_{i-1}-2S_i+S_{i+1}}{(\Delta\eta)^2} + \frac{S_{i-1}-2S_i+S_{i+1}}{(\Delta\eta)^2}\right], \tag{29}$$

$$T_2 = \frac{\partial^2 T}{\partial \eta^2} = \frac{1}{2}\left[\frac{T_{i-1}-2T_i+T_{i+1}}{(\Delta\eta)^2} + \frac{T_{i-1}-2T_i+T_{i+1}}{(\Delta\eta)^2}\right]. \tag{30}$$

The finite difference regarding the third order is

$$\frac{\partial^3 S}{\partial \eta^3} = S_3 = \frac{S_{i+2}-2S_{i+1}+2S_{i-1}-S_{i-2}}{2(\Delta\eta)^3}, \tag{31}$$

$$\frac{\partial^3 T}{\partial \eta^3} = T_3 = \frac{T_{i+2}-2T_{i+1}+2T_{i-1}-T_{i-2}}{2(\Delta\eta)^3}. \tag{32}$$

The finite difference regarding the fourth order is described as

$$\frac{\partial^4 S}{\partial \eta^4} = S_4 = \frac{S_{i+2}-4S_{i+1}+6S_i-4S_{i-1}-S_{i-2}}{(\Delta\eta)^4}, \tag{33}$$

$$\frac{\partial^4 T}{\partial \eta^4} = T_4 = \frac{T_{i+2}-4T_{i+1}+6T_i-4T_{i-1}-T_{i-2}}{(\Delta\eta)^4}. \tag{34}$$

The discretization procedure is obtained for $i = 2, 3 \ldots m-2$ as

$$\frac{S_{i+2}-2S_{i+1}+2S_{i-1}-S_{i-2}}{2(\Delta\eta)^3} + \left(\frac{\nu_f}{\nu_{Tetra}}T\frac{1}{2}\left[\frac{S_{i-1}-2S_i+S_{i+1}}{(\Delta\eta)^2} + \frac{S_{i-1}-2S_i+S_{i+1}}{(\Delta\eta)^2}\right]\right)$$

$$-\frac{\nu_f}{\nu_{Tetra}}\left(\frac{S_{i+1}-S_i}{\Delta\eta}\right)^2-\frac{2We\left(\frac{S_{i+1}-S_i}{\Delta\eta}\right)\frac{1}{2}\left[\frac{S_{i-1}-2S_i+S_{i+1}}{(\Delta\eta)^2}+\frac{S_{i-1}-2S_i+S_{i+1}}{(\Delta\eta)^2}\right]}{(1-\omega_1)^{2.5}(1-\omega_3)^{2.5}(1-\omega_4)^{2.5}(1-\omega_2)^{2.5}}$$

$$\frac{-SWe\frac{S_{i+2}-4S_{i+1}+6S_i-4S_{i-1}-S_{i-2}}{(\Delta\eta)^4}}{(1-\omega_1)^{2.5}(1-\omega_3)^{2.5}(1-\omega_4)^{2.5}(1-\omega_2)^{2.5}}+\frac{\sigma_f}{\sigma_{Tetra}}M\left(E-\frac{\partial S}{\partial\eta}\right)+\frac{\nu_f}{\nu_{Tetra}}$$

$$+\frac{We\left(\frac{1}{2}\left[\frac{S_{i-1}-2S_i+S_{i+1}}{(\Delta\eta)^2}+\frac{S_{i-1}-2S_i+S_{i+1}}{(\Delta\eta)^2}\right]\right)^2}{(1-\omega_1)^{2.5}(1-\omega_3)^{2.5}(1-\omega_4)^{2.5}(1-\omega_2)^{2.5}}$$

$$\frac{\nu_f}{\nu_{Tetra}}CT\frac{1}{2}\left[\frac{S_{i-1}-2S_i+S_{i+1}}{(\Delta\eta)^2}+\frac{S_{i-1}-2S_i+S_{i+1}}{(\Delta\eta)^2}\right]=0, \tag{35}$$

$$\frac{T_{i+2}-2T_{i+1}+2T_{i-1}-T_{i-2}}{2(\Delta\eta)^3}+\frac{\nu_f}{\nu_{Tetra}}S\frac{1}{2}\left[\frac{T_{i-1}-2T_i+T_{i+1}}{(\Delta\eta)^2}+\frac{T_{i-1}-2T_i+T_{i+1}}{(\Delta\eta)^2}\right]$$

$$-\frac{We\left[2\frac{T_{i+1}-T_i}{\Delta\eta}\right]\frac{T_{i+2}-2T_{i+1}+2T_{i-1}-T_{i-2}}{2(\Delta\eta)^3}}{(1-\omega_1)^{2.5}(1-\omega_3)^{2.5}(1-\omega_4)^{2.5}(1-\omega_2)^{2.5}}+\frac{\nu_f}{\nu_{Tetra}}C$$

$$+\frac{WeT\frac{T_{i+2}-4T_{i+1}+6T_i-4T_{i-1}-T_{i-2}}{(\Delta\eta)^4}}{(1-\omega_1)^{2.5}(1-\omega_3)^{2.5}(1-\omega_4)^{2.5}(1-\omega_2)^{2.5}}++\frac{\sigma_f}{\sigma_{Tetra}}M\left(E-\frac{S_{i+1}-S_i}{\Delta\eta}\right)$$

$$+\frac{We\left(\frac{1}{2}\left[\frac{T_{i-1}-2T_i+T_{i+1}}{(\Delta\eta)^2}+\frac{T_{i-1}-2T_i+T_{i+1}}{(\Delta\eta)^2}\right]\right)^2}{(1-\omega_1)^{2.5}(1-\omega_3)^{2.5}(1-\omega_4)^{2.5}(1-\omega_2)^{2.5}}$$

$$+\frac{\nu_f}{\nu_{Tetra}}CS\frac{1}{2}\left[\frac{S_{i-1}-2S_i+S_{i+1}}{(\Delta\eta)^2}+\frac{S_{i-1}-2S_i+S_{i+1}}{(\Delta\eta)^2}\right]$$

$$-\frac{\nu_f}{\nu_{Tetra}}C\left(\frac{S_{i+1}-S_i}{\Delta\eta}\right)^2=0, \tag{36}$$

$$\frac{1}{2}\left[\frac{\Theta_{i-1}-2\Theta_i+\Theta_{i+1}}{(\Delta\eta)^2}+\frac{\Theta_{i-1}-2\Theta_i+\Theta_{i+1}}{(\Delta\eta)^2}\right]+\frac{k_{Tetra}(\rho c_p)_f}{k_f(\rho c_p)_{Tetra}}S\frac{\Theta_{i+1}-\Theta_i}{\Delta\eta}$$

$$+\frac{k_{Tetra}(\rho c_p)_f}{k_f(\rho c_p)_{Tetra}}CT\frac{\Theta_{i+1}-\Theta_i}{\Delta\eta}+\frac{k_f}{k_{Tetra}}H_sPr\Theta+\frac{k_f}{k_{Tetra}}\frac{Pr\lambda Q_{sr}}{k_r}EXP(-\lambda\eta)$$

$$+\frac{k_{Tetra}(\rho c_p)_f}{k_f(\rho c_p)_{Tetra}}Pr\beta(S+T)^2\left(\frac{1}{2}\left[\frac{\Theta_{i-1}-2\Theta_i+\Theta_{i+1}}{(\Delta\eta)^2}+\frac{\Theta_{i-1}-2\Theta_i+\Theta_{i+1}}{(\Delta\eta)^2}\right]\right)$$

$$+\frac{k_{Tetra}(\rho c_p)_f}{k_f(\rho c_p)_{Tetra}}Pr\beta(S+T)\left(\frac{S_{i+1}-S_i}{\Delta\eta}+\frac{T_{i+1}-T_i}{\Delta\eta}\right)\frac{\Theta_{i+1}-\Theta_i}{\Delta\eta}$$

$$-\frac{k_{Tetra}(\rho c_p)_f}{k_f(\rho c_p)_{Tetra}}Pr\beta H_sPr(S)\frac{\Theta_{i+1}-\Theta_i}{\Delta\eta}-\frac{k_{Tetra}(\rho c_p)_f}{k_f(\rho c_p)_{Tetra}}Pr\beta H_sPr(T)\frac{\Theta_{i+1}-\Theta_i}{\Delta\eta}=0. \tag{37}$$

The boundary condition is discretization form

$$\left.\begin{array}{c} S(0)=0, S_1(0)=0, S_1(\infty)=1, T(0)=0, T_1(0)=0 \\ S_1(0)=1, \Theta(0)=\delta\frac{K_{Tetra}}{K_f}\Theta_1(0)+1, \Theta(\infty)=0 \end{array}\right\}, \tag{38}$$

and

$$\left.\begin{array}{c} S(0)=0, \frac{F_1-F_0}{\Delta\eta}=S_1(0)=0=, S_1(\infty)=1, T(0)=0, T_1(0)=0 \\ \frac{F_1-F_0}{\Delta\eta}=S_1(0)=1, \Theta'(0)=-1, \Theta(\infty)=0 \end{array}\right\}. \tag{39}$$

For i = 0, 1, 2,… m - 1, the discretized form of the skin friction coefficients and Nusselt numbers can be expressed as

$$-Re^{\frac{1}{2}}C_f=\frac{(1-3We)}{(1-\omega_2)^{2.5}(1-\omega_1)^{2.5}(1-\omega_3)^{2.5}(1-\omega_4)^{2.5}}\frac{\partial^2 \mathrm{S}}{\partial\eta^2}\Big|_{i=0,m}, \tag{40}$$

$$-Re^{\frac{1}{2}}C_g=\frac{(1-3We)}{(1-\omega_2)^{2.5}(1-\omega_1)^{2.5}(1-\omega_3)^{2.5}(1-\omega_4)^{2.5}}\frac{\partial^2 \mathrm{T}}{\partial\eta^2}\Big|_{i=0,m}, \tag{41}$$

$$Re^{\frac{-1}{2}}Nu=-\frac{k_f}{k_{Tetra}}\frac{\Theta_{i+1}-\Theta_i}{\Delta\eta}\Big|_{i=0,m}. \tag{42}$$

Here, $i=0,1,2\ldots m$. Here, $\Delta\eta$ and i indicate space and mesh points related to intervals of spaces. Moreover, F_i, G_i, and Θ_i are called new velocity and temperature profiles, respectively. Additionally, the updated temperature and velocity profiles are denoted by F_i, G_i, and Θ_i. For a transient state flow, repeat this process. At some point, F, G, and Θ will converge to values that roughly correspond to the steady-state solution of equations. Using the difference equations, the skin friction coefficients and Nusselt have also been formed. Graphs have been used to show all the results and converge well for the specified values of the parameters involved in the system of ODEs.

4. Results and discussion

In this section, discussion of the results for various parameters named $\mathrm{We}, \mathrm{E}, \mathrm{M}$, and C on primary velocity (S') as well as secondary velocity (T') are carried out by Figures 3−10. The ranges of dimensionless parameters are $0.0 \leq We \leq 10, 0.0 \leq C \leq 8.0, 0.0 \leq M \geq 5.0, 0.0 \leq E \leq 7.9, -2.0 \leq H_s \leq 4.0, , 0.6 \leq Pr \leq 100, 0.0 \leq \lambda \leq 8.5, 0.0 \leq Q_{sr} \leq 6.9, 0.0 \leq \beta \leq 7.5, 0.0 \leq \delta \leq 7.6, 0.0 \leq \omega_4 \leq 0.4, 0.0 \leq \omega_3 \leq 0.45, 0.0 \leq \omega_1 \leq 0.75, , 0.0 \leq \omega_2 \leq 0.86$. It is noticed that dot curves reveal constant heat flux, and convective boundary constraints are revealed by dash-dot curves. Figures 3 and 4 are predicted the visualizations of the Weissenberg number for primary velocity (S') and secondary velocity (T'). From Figures 3 and 4, flow and motion are reduced due to applying higher numerical values of the Weissenberg number. The Weissenberg number is mathematically revealed as a multiplication of relaxation time and shear rate. Either the typical relaxation time decreases or the shear rate increases as the Weissenberg number rises. As a result, the velocity field rises. Furthermore, velocity curves for the case of constant heat flux are higher than velocity curves for the case of convective boundary constraints. It is a dimensionless number that is utilized to know the behavior of elasticity and viscosity. We is the ratio between elastic and viscous forces. The Weissenberg parameter is utilized for determining viscoelastic materials based on the rate of deformation and relaxation time. Relaxation time increases the Weissenberg number. Moreover, We enhancement leads to enhancements in the deformation rate. In the study of rheology, We is a dimensionless quantity that is used to describe the ratio of a material's elasticity to viscosity response to deformation.

It is expressed as the product of the shear rate and the relaxation time of the material. Higher We denote a greater preference for elastic behavior over viscous behavior. Therefore, velocity declines with higher We. The width and thickness of momentum boundary layers decline when the viscous force is inclined. The role of E (electric field number) on velocity curves along the y-axis and x-axis using CHF and CBCs is shown in Figures 5 and 6. An electric field number is a fundamental concept in both electromagnetism and physics. This concept is due to electrically charged particles facing a force. Electric fields can be static (not changing over time) or dynamic (changing over time), depending on whether positive or negative electric charges are present. It is noted that velocity fields become enhanced when the electric field number is enhanced. The charged particles present in a fluid, such as ions, experience a force as a result of their electric charge when an electric field is applied to the fluid. This force may affect how these charged particles move, which would then affect how the fluid behaves with enhancement. Further, the charged particle observes the electric force, which is an external force. Nanoparticles are accelerated given a force applied to them using Newton's second law of motion. The charged particles in this instance accelerate in the electric field's direction. The electric field number occurs in the dimensionless momentum equation while the electric field is directly proportional to the motion of nanoparticles. An enhancement in the electric field number results in an enhancement in the velocity field. Therefore, motion in both directions is inclined when the electric field number is increased. The prediction of the magnetic number is based on primary velocity (S') and secondary velocity (T') is shown in Figures 7 and 8. The concept of the electric field number is experienced by EMHD. The study of the dynamics of electrically conducting fluids in the presence of magnetic fields is the focus of electromagnetic hydrodynamics, also referred to as magnetohydrodynamics. The interaction between the electric and magnetic fields affects the behavior of such fluids. The Lorentz force provides a mathematical explanation for an increase in velocity in the context of increasing EMHD, which is generally understood to indicate an increase in the strength of the applied electromagnetic field. The force that a charged particle traveling through an electromagnetic field experiences is known as the Lorentz force. The Lorentz force acts on the charged particles in the fluid in the context of fluid dynamics and EMHD. A decrease in Lorentz force results in a velocity curve decline. An enhancement in acceleration is investigated against a change in the magnetic number. It was revealed that utilizing magnetic numbers is produced because of Lorentz force implementation on the surface. A magnetic field is placed on the surface along the perpendicular direction of the surface. Lorentz force is visualized as a negative force that appears to slow the force. Therefore, the velocity field declines when Lorenz's force is magnified. Velocity curves for the case of $\mathrm{M} = 0$ are higher than velocity curves for $\mathrm{M} \neq 0$. It is noticed that the case related to $M = 0$ is known as the case of hydrodynamics while the case related to $M \neq 0$ is called the magnetohydrodynamic case. The force that the magnetic field applies to the fluid is known as the Lorentz force and it is denoted by the symbol (B_0). Both the magnetic field and the current density are perpendicular to this force. This force acts in the opposite direction of the velocity, as indicated by the negative sign. The Lorentz force increases with an increase in the magnetic field. An increase in the Lorentz force is opposed to the fluid motion as a resistive force because it acts in the opposite direction of the velocity. The motion of nanoparticles in the case of hydrodynamics is higher than the motion in the case of magnetohydrodynamics. Hence, motion and momentum boundary layer thickness can be measured by variations in magnetohydrodynamic motion. The strength of the magnetic field is placed perpendicular to the direction of flow. Therefore, the flow declines when the Lorentz force is magnified. Figures 9 and 10 reveal an illustration of C on the velocity curves utilizing CHF and CBCs. Velocity curves increase

when C is enhanced in the presence of CHF and CBCs. Figures 11−14 predict the estimation of $\mathrm{C}, \mathrm{Q_{sr}}, \mathrm{H_s}$, and Ec on temperature curves utilizing CHF and CBCs. In these graphs, dot curves reveal constant heat flux and convective boundary constraints revealed by dash-dot curves. The prediction and change in C on the temperature curve are carried out in Figure 11 using CHF and CBCs. A declination role is visualized on the temperature curve when c is increased. Here, C is a dimensionless number and it is a noddle point number. It was investigated that noddle point number (C) has a directly proportional velocity field. An increment in the noddle point number leads to velocity fields in both directions being magnified. The velocity field for the case of $C = 0$ is less than the velocity fields for the case of $C > 0$. Figure 12 reveals the role of solar radiation number $(\mathrm{Q_{sr}})$ on the temperature curve. Solar radiation is predicted by the Stefan-Boltzmann equation, which has a relation between radiative heat flux to the surface temperature. $\mathrm{Q_{sr}}$ is a dimensionless number that occurs in the energy equation. Mathematically, $\mathrm{Q_{sr}}$ is a directly proportional temperature field. The temperature field inclines when $\mathrm{Q_{sr}}$ is enhanced. Variations in the temperature field is based on $\mathrm{Q_{sr}}$. Thickness associated with thermal layers can be managed using a variation of $\mathrm{Q_{sr}}$. The radiative heat flow is exactly proportional to the fourth power of the surface temperature, according to the Stefan-Boltzmann equation. As a result, a rise in temperature causes a notable rise in the radiative heat flow. The characterizations of heat sink $(\mathrm{H_s})$ on the temperature curve are addressed in Figure 13. $\mathrm{H_s}$ is known as a dimensionless parameter that is occulted due to a heat sink placed on the wall of temperature. It is an external heat source that is used for controlling heat energy in the motion of particles as well as temperature on the wall. Here, two types of heat energy are observed based on heat absorption and heat generation. Mathematically, it was determined that $\mathrm{H_s} > 0$ is known as heat generation while $\mathrm{H_s} < 0$ is termed heat absorption. From Figure 13, it was concluded that two kinds of behavior related to energy have been noticed. Furthermore, temperature curves for large values of $\mathrm{H_s}$ increase when $\mathrm{H_s}$ is increased. The rate of heat generation per unit volume within the material is represented by the heat source term Q_0. An increase in Q_0 indicates a higher rate of heat generation per unit volume, which raises the system's energy input rate. From a mathematical perspective, raising Q_0 has a direct impact on the equation for heat conduction on the right side. Therefore, thermal energy is enhanced concerning higher values of the heat source number. This is due to an external heat energy source being placed on the surface. Figure 14 exhibits the role of Ec on the temperature field. Ec is termed a dimensionless number that occurs using the concept of viscous dissipation in the energy equation. This increasing role of temperature distribution is due to a rise in Eckert number indicating that the fluid has more kinetic energy than is being transported in terms of enthalpy. When the Eckert number is magnified, the temperature rises. The coefficient of viscous dissipation and Joule heating occurs due to the Eckert number. An increase in the Eckert number indicates that the heat dissipated as a result of the interaction between the Joule heating process and frictional forces has increased. A change in the specific heat in the flow leads to increased fluid velocities or a decrease in the transit of enthalpy. The nature of the fluid and the heat produced by viscous forces during flow are related to the impact of viscous dissipation in nanofluids. When internal friction within the fluid causes mechanical energy to be transformed into heat, it is known as viscous dissipation. The presence of nanoparticles can improve the heat dissipation properties of nanofluids, which are suspensions of nanoparticles in a base fluid as shown in Figure 15. Figure 16 explores the role of We and M on the skin friction coefficient given the contour graph. It was visualized that higher values of We and M make inclinations of the skin friction coefficient. The skin friction coefficient is based on the changes in flow dynamics brought on by an increase in the magnetic Reynolds number. Electrically conductive fluids

and magnetic fields can interact, and this interaction can affect the fluid's flow characteristics. Figure 17 estimates E and c on divergent velocity. The influence of magnetic forces on fluid flow is increased when magnetic field strength increases, which raises the skin friction coefficient. Concurrently, an increase in the Weissenberg number indicates a higher material reaction to flow deformation, which adds to the elevated skin friction coefficient. The opposite treatment is visualized on skin friction coefficient versus higher values of E and c. The distribution of the Nusselt number against the distribution of Ec and c is carried out in Figure 18. The characterizations of c and Q_{sr} on the Nusselt number have been addressed in Figure 19. Dimensionless parameters, called the Nusselt number and the Eckert number, are used in fluid dynamics and heat transfer to describe various aspects of heat transfer processes. The fluid's kinetic energy is related to the Eckert number, whereas the Nusselt number is related to convective heat transfer. Nusselt number is a dimensionless number that is used to describe the proportion of conductive to convective heat transfer across a boundary. Nusselt number is directly proportional to the change in heat source number. Therefore, the temperature gradient is magnified. A declination trend in temperature distribution is visualized in Figure 19. Table 2 reveals illustration of various parameters H_s, E, C, We and M between tera hybrid nanofluid Al_2O_3-Fe_3O_4/EO, Al_2O_3-Fe_3O_4-Cu/EO tri-hybrid nanofluid Al_2O_3-Fe_3O_4/EO, Al_2O_3-Fe_3O_4/EO and hybrid nanofluid Al_2O_3-Fe_3O_4/EO, Al_2O_3/EO. From Table 2, it was predicted that the heat transfer rate for Al_2O_3-Fe_3O_4/EO, Al_2O_3-Fe_3O_4-Cu/EO is higher than the heat transfer rate for Al_2O_3-Fe_3O_4/EO, Al_2O_3-Fe_3O_4/EO. The ratio of convective to conductive heat transfer across a boundary is measured using the dimensionless Nusselt number, which is used in fluid dynamics and heat transfer. The rate of heat energy declined against the declination of H_s, E, C, and M but the inclination of the temperature gradient is enhanced when We is enhanced. For higher values of heat source number, the Nusselt number declines because the temperature gradient is inversely proportional to the heat source number. An increase in the Nusselt number results in a temperature gradient. The Nusselt number declines with higher values of the magnetic number because convective heat transfer is suppressed, and the Nusselt number decreases as the magnetic field number increases. The fluid flow can be altered by Lorentz forces induced by the magnetic field. The convective heat transfer coefficient may drop, lowering the Nusselt number. The dynamics of heat transfer can be impacted by the electric field's influence on the boundary layer. The convective heat transfer coefficient brings a change in the Nusselt number, which can be affected by modifications to the boundary layer.

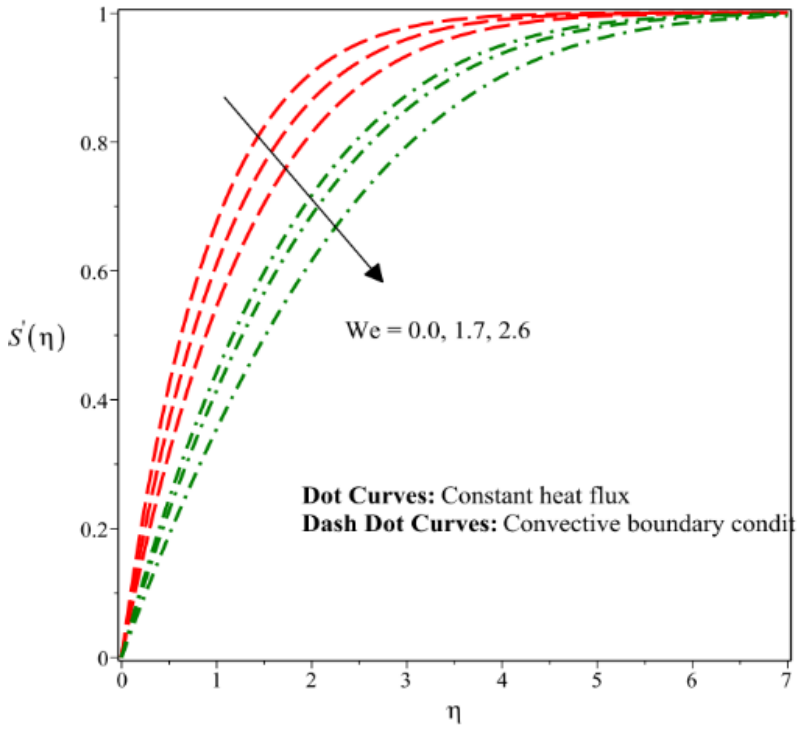

Figure 3. Influence of Weissenberg number on velocity field (in x-direction) for convective boundary conditions and constant heat flux when $\mathrm{C}=-3.0, M=0.32, E=2.0, H_s=-3, Pr=3.0, \lambda=5.0, Q_{sr}=-3.2, \beta=2.0, \delta=0.3$.

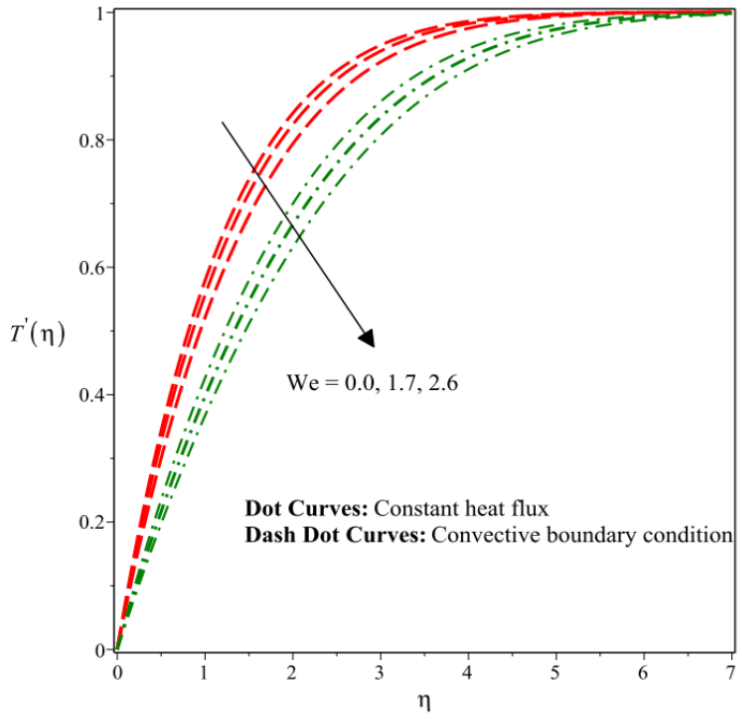

Figure 4. Influence of Weissenberg number on velocity field (in y-direction) for convective boundary conditions and constant heat flux when $\mathrm{C}=0.5, M=0.01, E=3.0, H_s=-5, Pr=3.0, \lambda=5.0, Q_{sr}=-3.2, \beta=2.0, \delta=0.3$.

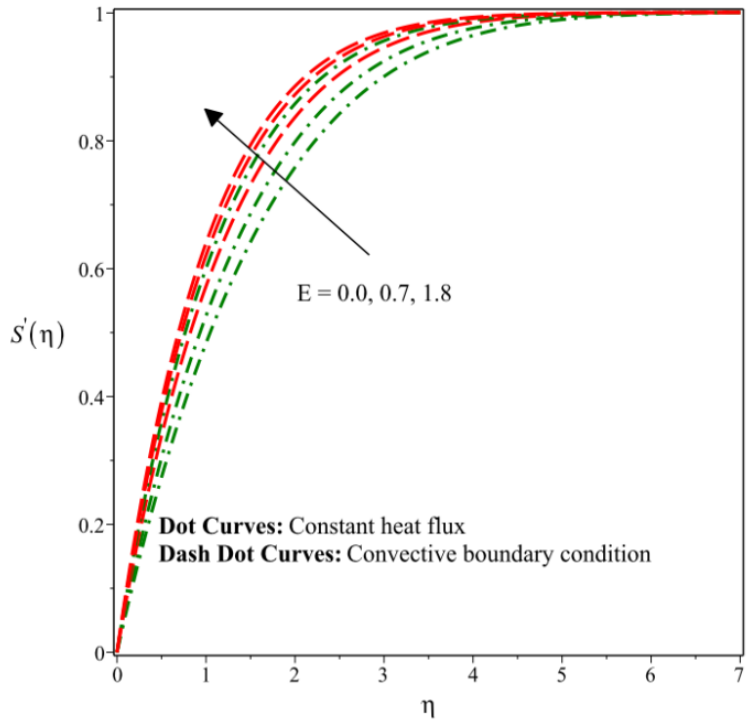

Figure 5. Influence of electric field number on velocity field (in the x-direction) for convective boundary conditions and constant heat flux when $We = 5.0, C = -2.0, M = 0.2, H_s = -3, Pr = 3.0, \lambda = 3.0, Q_{sr} = -3.2, \beta = 1.03, \delta = 0.5$.

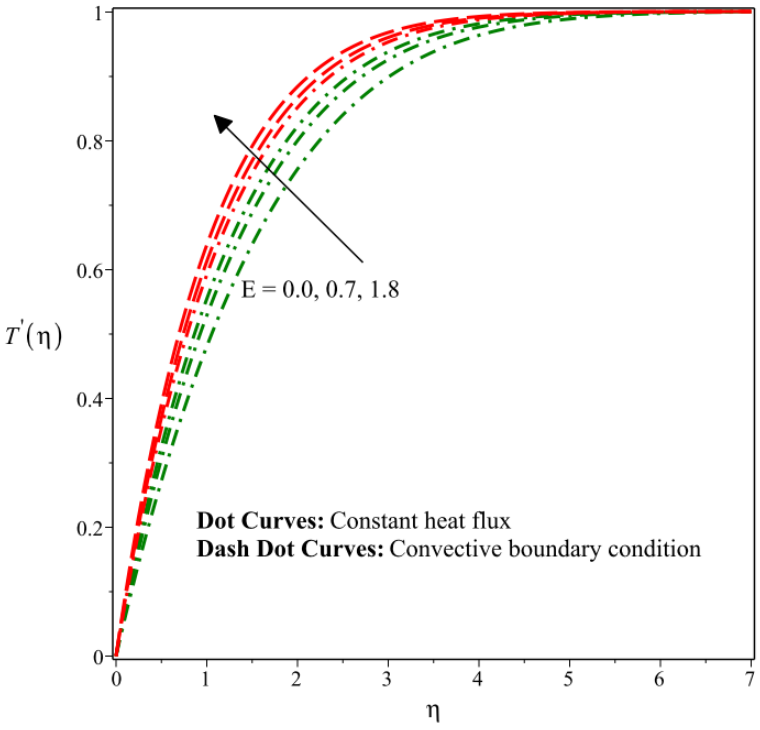

Figure 6. Influence of electric field number on velocity field (in y-direction) for convective boundary conditions and constant heat flux when $We = 5.0, C = -2.0, M = 0.2, H_s = -3, Pr = 3.0, \lambda = 3.0, Q_{sr} = -3.2, \beta = 1.03, \delta = 0.5$.

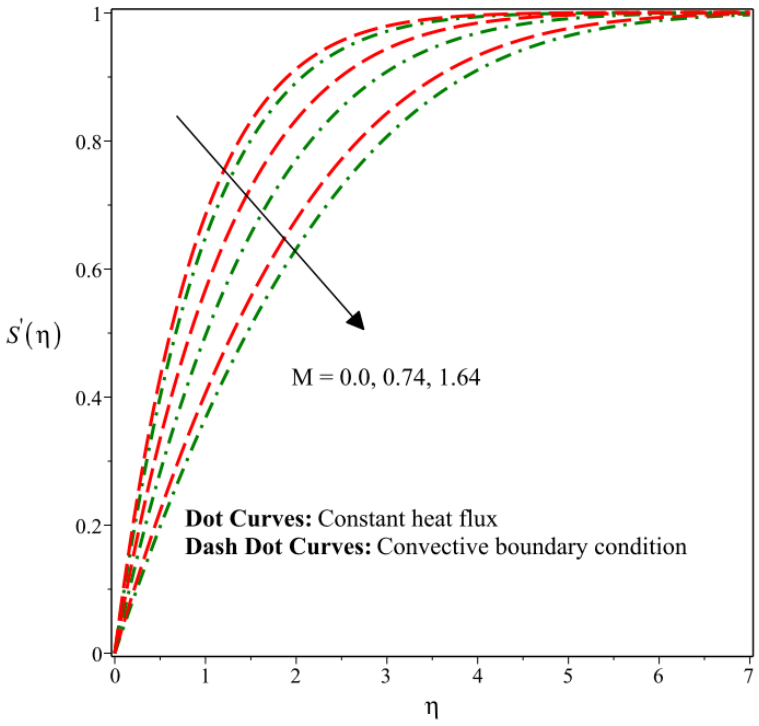

Figure 7. Influence of magnetic field number on velocity field (in x-direction) for convective boundary conditions and constant heat flux when $We = 5.0, C = 0.2, E = 2.0, H_s = -5, Pr = 3.0, \lambda = 7.0, Q_{sr} = 2.0, \beta = 3.0, \delta = 0.3$.

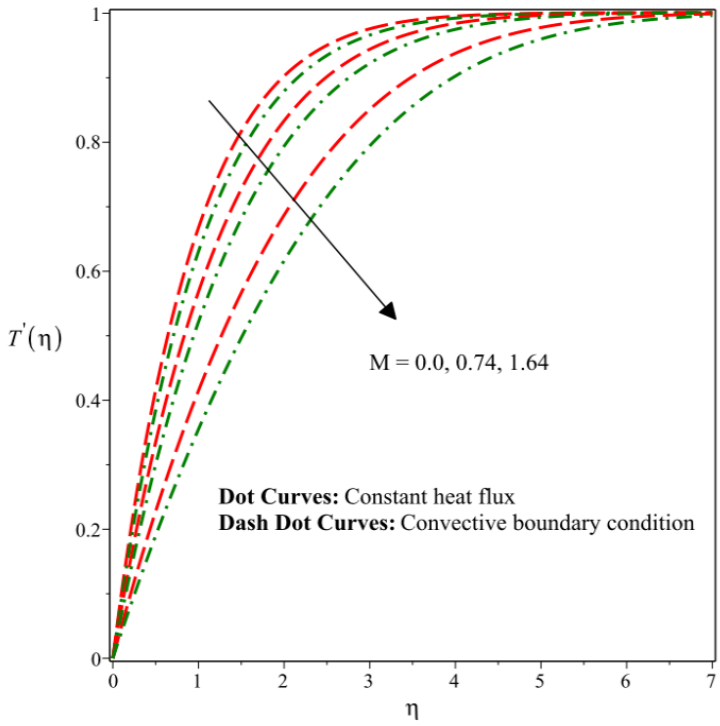

Figure 8. Influence of magnetic field number on velocity field (in y-direction) for convective boundary conditions and constant heat flux when $We = 5.0, C = 0.2, E = 2.0, H_s = -5, Pr = 3.0, \lambda = 7.0, Q_{sr} = 2.0, \beta = 3.0, \delta = 0.3$.

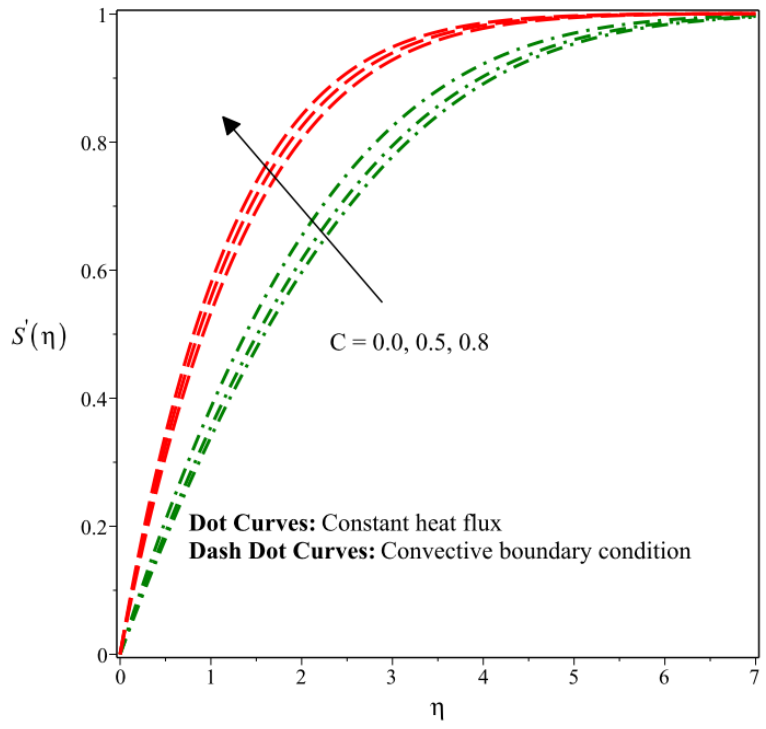

Figure 9. Influence of noddle point number on velocity field (in x-direction) for convective boundary conditions and constant heat flux when $We = 3.5, M = 0.3, E = 3.0, H_s = -5, Pr = 7.0, \lambda = 5.0, Q_{sr} = 3.0, \beta = 7.0, \delta = 2.6$.

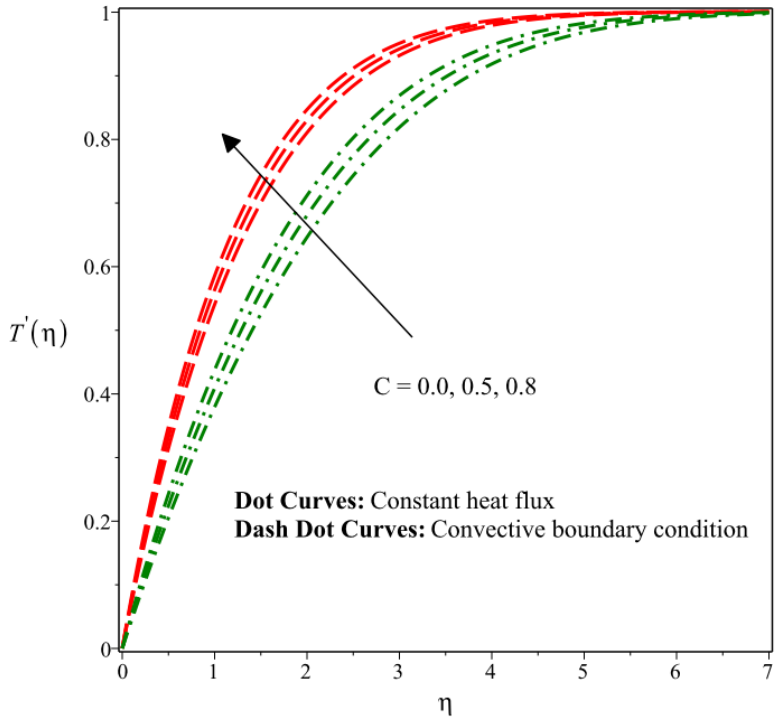

Figure 10. Influence of noddle point number on velocity field (in y-direction) for convective boundary conditions and constant heat flux when $We = 3.5,\ M = 0.3, E = 3.0, H_s = -5, Pr = 7.0, \lambda = 5.0, Q_{sr} = 3.0, \beta = 7.0, \delta = 2.6$.

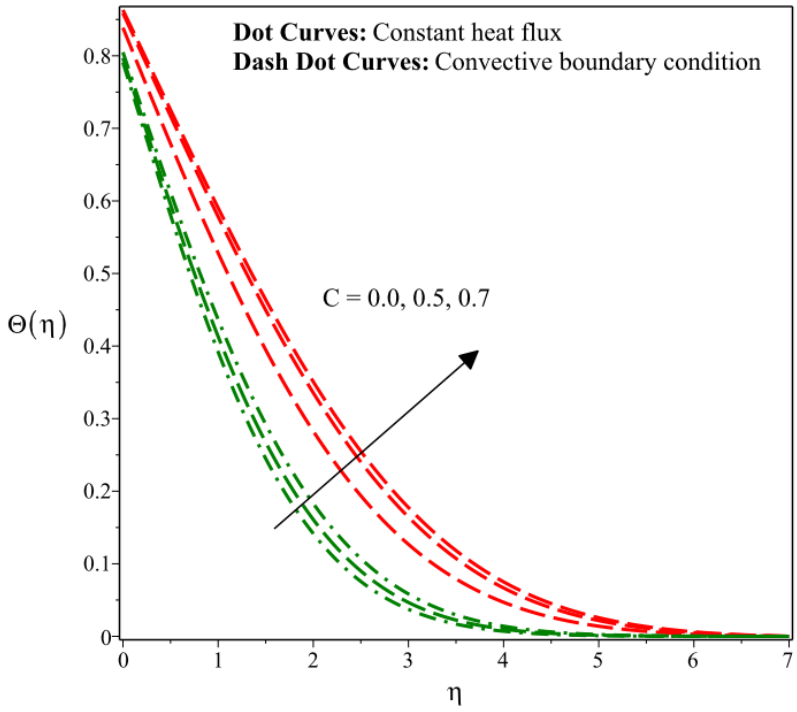

Figure 11. Influence of noddle point number on temperature field for convective boundary conditions and constant heat flux when $We = 2.0 M = 0.3, E = 2.0, H_s = 2.4, Pr = 3.0, \lambda = 5.0, Q_{sr} = 5.0, \beta = 2.0, \delta = 2.3$.

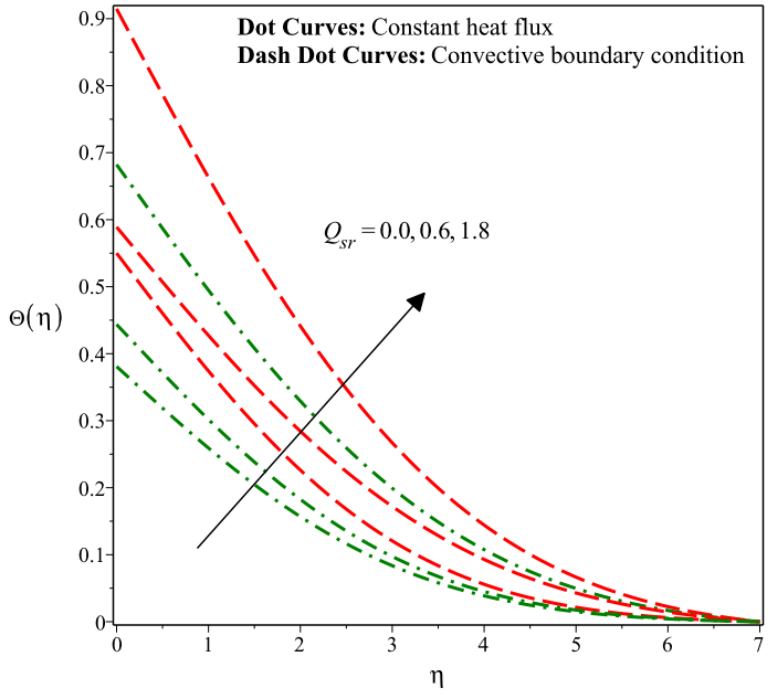

Figure 12. Influence of solar radiation number on temperature field for convective boundary conditions and constant heat flux when $We = 5.0, C = -3.0, M = 0.32, E = 2.0, H_s = 3.5, Pr = 3.0, \lambda = 5.0 \beta = 4.0, \delta = 0.3$.

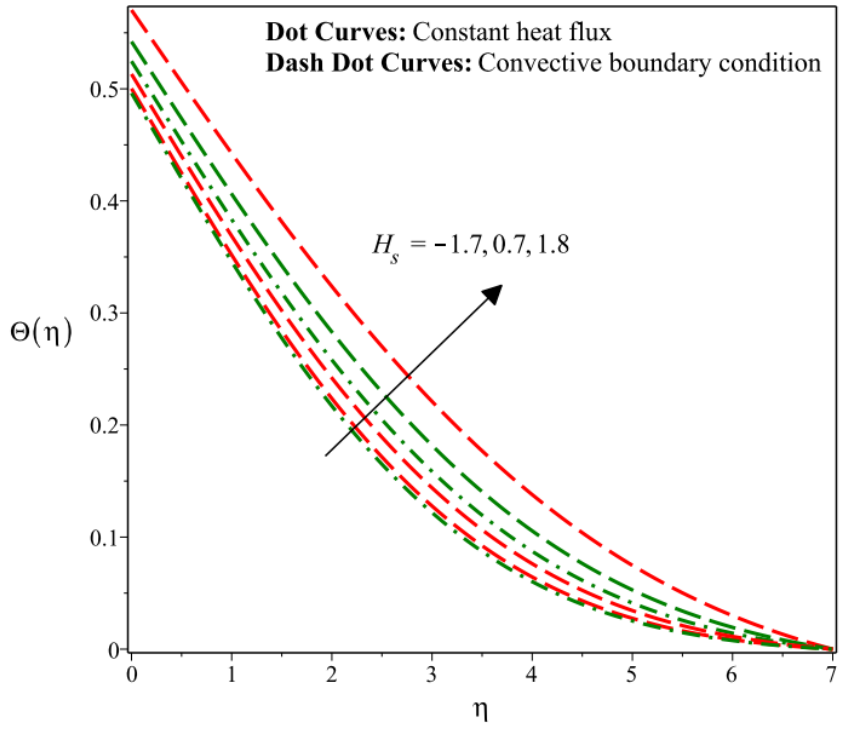

Figure 13. Influence of heat source number on temperature field for convective boundary conditions and constant heat flux when $We = 1.3, C = -2.0, M = 4.5, E = 3.0, H_s = -5, Pr = 7.0, \lambda = 5.0, Q_{sr} = -3.2, \beta = 2.0, \delta = 0.3$.

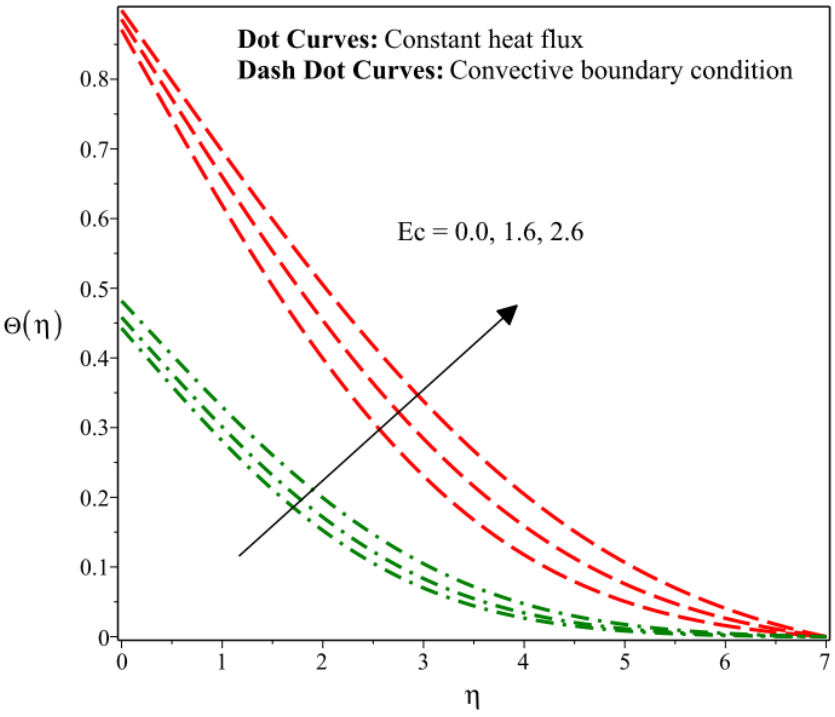

Figure 14. Influence of Eckert number on temperature field for convective boundary conditions and constant heat flux when $We = 3.0, C = -7.0, M = 0.32, E = 3.0, H_s = 0.4, Pr = 7.0, \lambda = 5.0, Q_{sr} = 3.4, \beta = 2.0, \delta = 0.3$.

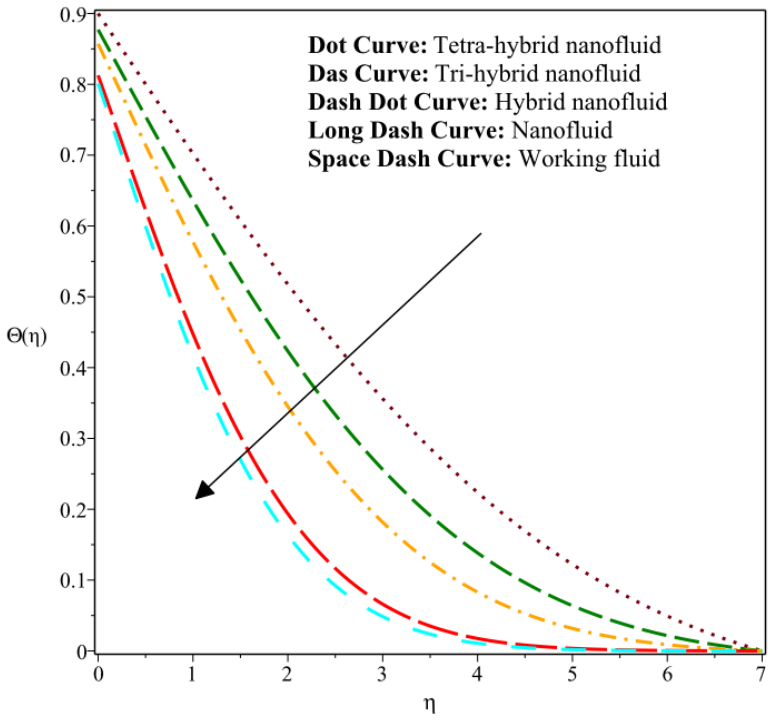

Figure 15. Comparative Outcomes between working fluid, hybrid nanofluid, tera-hybrid nanofluid and ternary hybrid nanofluid when $We = 7.0, C = 3.0, M = 0.32, E = 2.0, H_s = -3, Pr = 3.0, \lambda = 5.0, Q_{sr} = -3.2, \beta = 2.0, \delta = 0.5$.

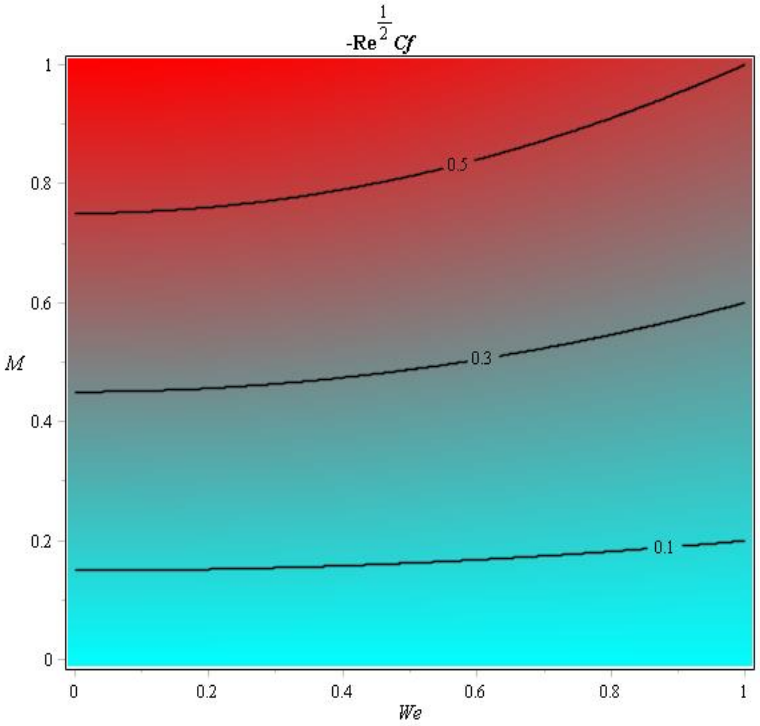

Figure 16. Comparative outcomes of magnetic field and Weissenberg numbers on skin friction coefficient when $We = 3.0, C = 3.0, M = 0.2, E = 2.0, H_s = -3, Pr = 3.0, \lambda = 5.0, Q_{sr} = -3.2, \beta = 2.0, \delta = 1.3$.

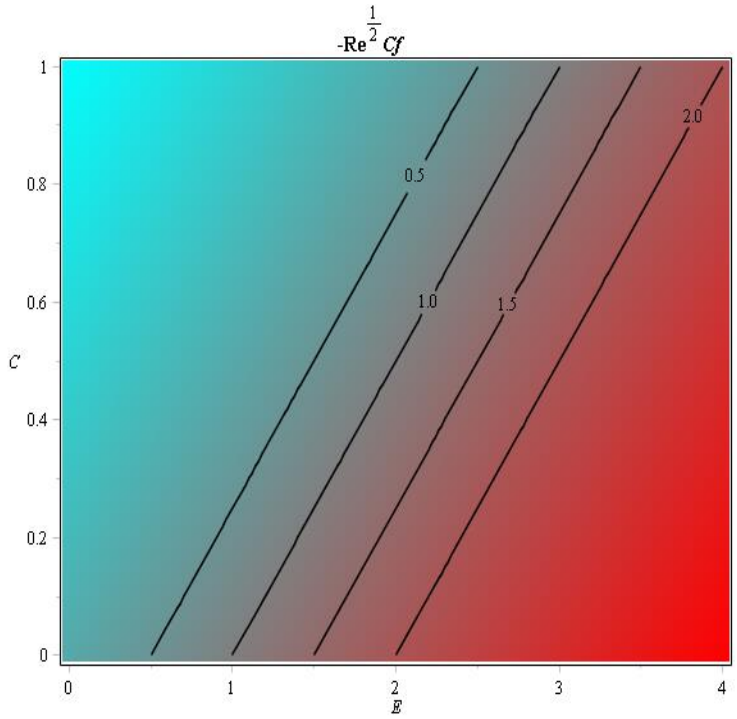

Figure 17. Comparative outcomes of electric field and noddle point numbers on skin friction coefficient when $We = 3.0, C = -3.0, M = 0.3, E = 2.0, H_s = -7, Pr = 6.0, \lambda = 5.0, Q_{sr} = -5.2, \beta = 2.0, \delta = 0.3$.

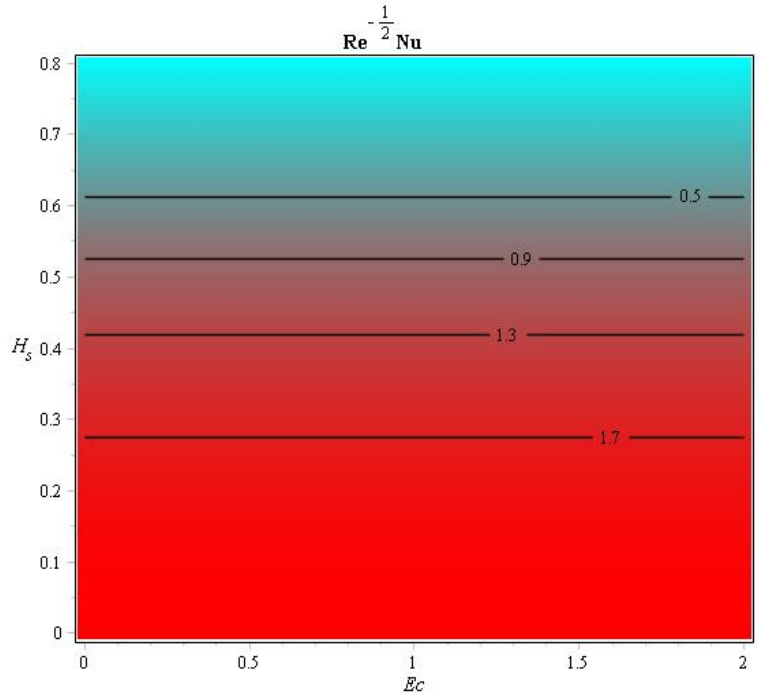

Figure 18. Comparative outcomes of Eckert and heat source numbers on Nusselt number when $We = 6.0, C = 3.0, M = 2.32, E = 2.0, H_s = -3.6, Pr = 7.0, \lambda = 5.0, Q_{sr} = 3.7, \beta = 3.0, \delta = 0.3$.

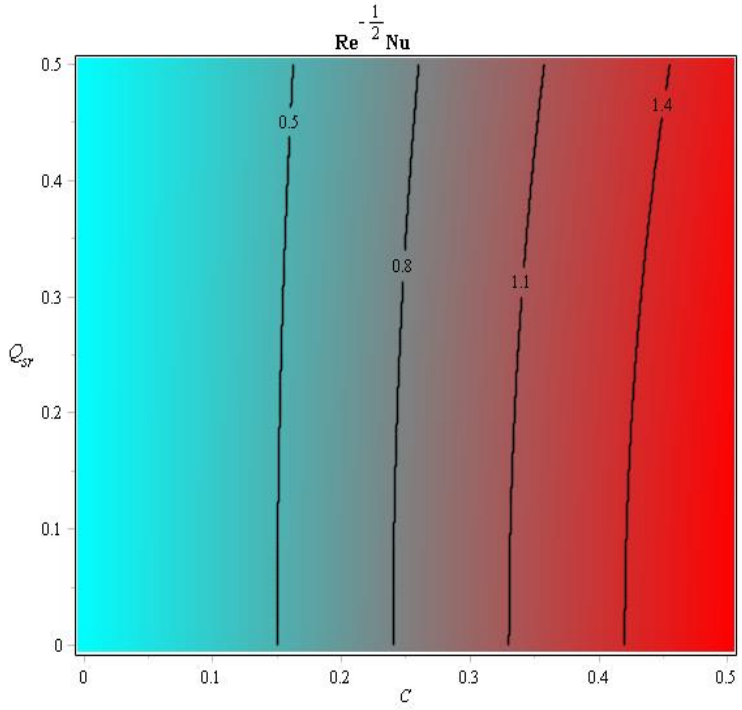

Figure 19. Comparative outcomes Eckert and heat source numbers when $We = 3.0, C = 2.0, M = 0.3, E = 2.0, H_s = -3, Pr = 3.0, \lambda = 5.0, Q_{sr} = -5.0, \beta = 2.0, \delta = 0.3$.

Table 2. Comparative simulations among Al_2O_3-Fe_3O_4/EO, Al_2O_3-Fe_3O_4-Cu/EO and Al_2O_3 - Fe_3O_4 - Cu - TiO_2 /EO on Nusselt number when $We = 3.0, C = -3.0, M = 0.32, E = 2.0, H_s = -3, Pr = 3.0, \lambda = 5.0, Q_{sr} = -3.2, \beta = 2.0, \delta = 0.3$.

		Al_2O_3-Fe_3O_4/EO	Al_2O_3-Fe_3O_4-Cu/EO	Al_2O_3-Fe_3O_4-Cu-TiO_2/EO
		$Re^{\frac{-1}{2}}Nu$	$Re^{\frac{-1}{2}}Nu$	$Re^{\frac{-1}{2}}Nu$
	−2.0	0.2431157370	1.04117802461	2.2847120984
H_s	0.6	0.2355292920	1.03069072115	2.1227628846
	1.5	0.2100296982	1.01579475033	2.1131790013
	0.0	0.3317954914	1.04020353189	2.1608141276
E	0.6	0.3110955080	1.03406598637	2.1462639455
	1.4	0.3081959450	1.02748633898	2.1399453559
	0.0	0.3833488662	1.05054143034	2.5021657214
C	1.3	0.3767862010	1.04328993974	2.2131597590
	1.5	0.3087171768	1.02577784604	2.1231113842
	0.0	0.4493279178	1.05804190847	2.2321676339
We	1.7	0.4587823450	1.06011198013	2.2404479205
	2.0	0.4772238188	1.08201264220	2.2780505687
	0.0	0.4447771272	1.06376435390	2.2550574156
M	0.53	0.4315505690	1.06238432034	2.2415372814
	0.85	0.4104502672	1.06159856465	2.2003942586

5. Conclusions

The current computational analysis is based on tetra-hybrid nano-structures and non-Fourier's law for better improvement of heat energy over a circular cylinder utilizing solar thermal radiation and heat sink. Two kinds of boundary conditions based on constant heat flux and convective boundary conditions are utilized in the presence of EMH flow. The current study highlights vital aspects of the maximum production of heat energy in the industrial field. The key findings are displayed below.

1) The thermal performance achieved by tera-hybrid nano-fluid is greater than the thermal performance achieved by hybrid nano-fluid, nanofluid, and working fluid. Such phenomena are applicable in modern coolants to improve heat dissipation in electronics, aerospace systems' performance, and solar thermal collectors, which improve solar energy capture and storage efficiency.
2) The temperature field increases by increasing impacts of heat source, solar radiation, noddle point, and Eckert numbers for the cases of constant heat flux and convective boundary conditions. Higher temperature enhances the thermal performance of solar collectors and solar energy systems as well as the efficiency of solar thermal power plants and solar water heaters.
3) The velocity field declines when magnetic field and Weissenberg numbers are enhanced but the velocity field increases when noddle point and electric field numbers are enhanced. In magnetohydrodynamic systems, higher velocities in conductive fluids can result in more efficient power generation.
4) The fluid temperature gradually dissipates to the surroundings due to the declined convective heat transfer in convective boundary conditions, and the constant heat flux magnitude is higher than the convective boundary conditions magnitude. Higher constant heat flux may be advantageous for solar thermal collectors, which turn sunlight into heat.
5) Certain aspects of the heat transfer process are implied when the Nusselt number, which measures the rate of heat transfer, decreases as the values of solar radiation, C, heat source, and Eckert number increase. A decreasing Nusselt number as Eckert number rises could indicate difficulties in removing heat from these flows.
6) Momentum boundary layers (associated with width and thickness) for the case of terra-hybrid nanostructures are higher than momentum boundary layers (associated with width and thickness) for the case of tri-hybrid nanomaterials and nanomaterials.
7) Nusselt number becomes significant for the case of Al_2O_3-Fe_3O_4-Cu-TiO_2/EO than for the cases of Al_2O_3-Fe_3O_4-Cu/EO and Al_2O_3-Fe_3O_4/EO.
8) Momentum boundary layers (associated with thickness) for the case of $We = 0$ are higher than momentum boundary layers (associated with thickness) for the case of $We > 0$.
9) Improved heat transfer, solar thermal systems, refrigeration, electronics cooling, medical applications, aerospace industries, energy storage, solar systems, and electronic systems are among the fields that benefit from this research. Enhancing heat transfer leads to improved energy storage device performance, which advances the integration of renewable energy sources. Improved heat transfer is advantageous for solar-powered devices, concentrating solar technologies and advanced solar panels.

Future recommendation: The current study is based on Walters'-B fluid containing tetra-hybrid nano-fluid over a circular cylinder in the presence of a heat source, magnetic field, solar thermal radiation, convective heat flux, and constant heat flux. Additional non-Newtonian fluids problems include Herschel-Bulkley fluids, Bingham plastic, and the Second-Grade fluid model. These models can also be used to model and analyze the current investigation. Under certain circumstances,

conservation laws with intricate colocations will address the intricacy of the problems. Because of accuracy, the finite element method's implementation is difficult. We intend to apply the finite element method to PDEs in the future. All things considered, the current study provides a strong basis for future efforts to apply non-Fourier's theory and tetra-hybrid nanofluid to improve thermal enhancement and cooling performance.

Use of AI tools declaration

The authors declare that they have not used Artificial Intelligence (AI) tools in the creation of this article.

Acknowledgments

The authors present their appreciation to King Saud University for funding this research through the Researchers Supporting Program number (RSPD2024R704), King Saud University, Riyadh, Saudi Arabia.

This work was partially supported by Science and Technology General Project of Jiangxi Provincial Department of Education (No. GJJ2203204).

Conflict of interest

The authors declare no conflict of interest.

References

1. A. Shafiq, Z. Hammouch, H. F. Oztop, *Radiative MHD flow of third-grade fluid towards a stretched cylinder*, In: 4th International Conference on Computational Mathematics and Engineering Sciences (CMES-2019), Springer International Publishing, **4** (2020), 166−185. https://doi.org/10.1007/978-3-030-39112-6_12
2. H. Vaidya, R. Choudhari, F. Mebarek-Oudina, I. L. Animasaun, K. V. Prasad, O. D. Makinde, Combined effects of homogeneous and heterogeneous reactions on peristalsis of Ree-Eyring liquid: Application in hemodynamic flow, *Heat Transf.*, **50** (2021), 2592−2609. https://doi.org/10.1002/htj.21995
3. A. Shafiq, F. Mebarek-Oudina, T. N. Sindhu, G. Rasool, Sensitivity analysis for Walters-B nano liquid flow over a radiative Riga surface by RSM, *Sci. Iran.*, **29** (2022), 1236−1249. https://doi.org/10.24200/sci.2021.58293.5662
4. I. Khan, F. Ali, N. A. Shah, Interaction of magnetic field with heat and mass transfer in free convection flow of a Walters'-B fluid, *Eur. Phys. J. Plus*, **131** (2016), 77. https://doi.org/10.1140/epjp/i2016-16077-7
5. T. Hayat, A. Shafiq, M. Mustafa, A. Alsaedi, Boundary-layer flow of Walters' B fluid with Newtonian heating, *Z. Naturforsch. A*, **70** (2015), 333−341. https://doi.org/10.1515/zna-2014-0280
6. Q. Al-Mdallal, K. A. Abro, I. Khan, Analytical solutions of fractional Walter's B fluid with applications, *Complexity*, **2018** (2018), 1−10. https://doi.org/10.1155/2018/8131329
7. A. Tanveer, M. Khan, T. Salahuddin, B. Al Alwan, A. Amari, Dynamics of Walters' B fluid due to periodic wave in a convectively heated channel with internal heat generation, *Math. Comput. Simul.*, **199** (2022), 374−393. https://doi.org/10.1016/j.matcom.2022.03.018

8. R. Mahat, M. Saqib, I. Khan, S. Shafie, N. A. M. Noor, Thermal radiation effect on Viscoelastic Walters'-B nanofluid flow through a circular cylinder in convective and constant heat flux, *Case Stud. Therm. Eng.*, **39** (2022), 102394. https://doi.org/10.1016/j.csite.2022.102394
9. N. A. Shah, K. A. Abro, I. Siddique, Thermography of ferromagnetic Walter's-B fluid thermal stratification, *South Afr. J. Chem. Eng.*, **36** (2021), 118−126. https://doi.org/10.1016/j.sajce.2020.12.004
10. A. B. Johnson, B. I. Olajuwon, Impact of radiation and heat generation/absorption in a Walters' B fluid through a porous medium with thermal and thermo diffusion in the presence of chemical reaction, *Int. J. Model. Simul.*, **43** (2023), 87−100. https://doi.org/10.1080/02286203.2022.2035948
11. P. K. Asifa, T. Anwar, Z. Shah, W. Watthayu, Analysis and modeling of fractional electro-osmotic ramped flow of chemically reactive and heat absorptive/generative Walters' B fluid with ramped heat and mass transfer rates, *AIMS Math.*, **6** (2021), 5942−5976. https://doi.org/10.3934/math.2021352
12. A. Shafiq, A. B. Çolak, T. N. Sindhu, Optimization of bioconvective magnetized Walter's B nanofluid flow towards a cylindrical disk with artificial neural networks, *Lubricants*, **10** (2022), 209. https://doi.org/10.3390/lubricants10090209
13. M. I. Khan, F. Alzahrani, Activation energy and binary chemical reaction effect in nonlinear thermal radiative stagnation point flow of Walter-B nanofluid: Numerical computations, *Int. J. Mod. Phys. B*, **34** (2020), 2050132. https://doi.org/10.1142/S0217979220501325
14. C. K. Damala, V. Bhumarapu, O. D. Makinde, Radiative MHD Walter's liquid-B flow past a semi-infinite vertical plate in the presence of viscous dissipation with a heat source, *Eng. T.*, **69** (2021), 373−401. https://doi.org/10.24423/EngTrans.1370.20211215
15. G. P. Vanitha, U. S. Mahabaleshwar, Z. Liu, X. Yang, B. Sundén, Magnetohydrodynamic Marangoni boundary layer flow of nanoparticles with thermal radiation and heat transfer in a porous sheet, *Case Stud. Therm. Eng.*, **44** (2023), 102815. https://doi.org/10.1016/j.csite.2023.102815
16. H. Waqas, M. Alghamdi, T. Muhammad, M. A. Khan, Bioconvection transport of magnetized Walter's B nanofluid across a cylindrical disk with nonlinear radiative heat transfer, *Case Stud. Therm. Eng.*, **26** (2021), 101097. https://doi.org/10.1016/j.csite.2021.101097
17. O. D. Makinde, M. G. Reddy, K. V. Reddy, Effects of thermal radiation on MHD peristaltic motion of Walters-B fluid with heat source and slip conditions, *J. Appl. Fluid Mech.*, **10** (2017), 1105−1112. https://doi.org/10.18869/acadpub.jafm.73.241.27082
18. M. V. Krishna, Hall and ion slip effects on MHD laminar flow of an elastico-viscous (Walter's-B) fluid, *Heat Transf.*, **49** (2020), 2311−2329. https://doi.org/10.1002/htj.21722
19. G. Chakraborty, P. R. Sengupta, *MHD flow of unsteady viscoelastic (Walters liquid B') conducting fluid between two porous concentric circular cylinders*, In: Proceedings of the National Academy of Sciences, Section A: Physical Sciences, India, **64** (1994).
20. P. Y. Huang, J. Feng, Wall effects on the flow of viscoelastic fluids around a circular cylinder, *J. Non-Newton. Fluid*, **60** (1995), 179−198. https://doi.org/10.1016/0377-0257(95)01394-2
21. G. M. Moatimid, M. H. Zekry, Nonlinear stability of electro-visco-elastic Walters' B type in porous media, *Microsyst. Technol.*, **26** (2020), 2013−2027. https://doi.org/10.1007/s00542-020-04752-6
22. A. R. M. Kasim, N. F. Mohammad, S. Shafie, *Effect of heat generation on free convection boundary layer flow of a viscoelastic fluid past a horizontal circular cylinder with constant surface heat flux*, In: AIP Conference Proceedings, American Institute of Physics, **1450** (2012), 286−292.

23. S. Nadeem, N. S. Akbar, Influence of heat and chemical reactions on Walter's B fluid model for blood flow through a tapered artery, *J. Taiwan Inst. Chem. Eng.*, **42** (2011), 67−75. https://doi.org/10.1016/j.jtice.2010.03.012
24. R. P. Bharti, R. P. Chhabra, V. Eswaran, Steady flow of power law fluids across a circular cylinder, *Can. J. Chem. Eng.*, **84** (2006), 406−421. https://doi.org/10.1002/cjce.5450840402
25. R. Naz, S. Tariq, H. Alsulami, Inquiry of entropy generation in stratified Walters' B nanofluid with swimming gyrotactic microorganisms, *Alex. Eng. J.*, **59** (2020), 247−261. https://doi.org/10.1016/j.aej.2019.12.037
26. M. I. Khan, M. Tamoor, T. Hayat, A. Alsaedi, MHD boundary layer thermal slip flow by nonlinearly stretching cylinder with suction/blowing and radiation, *Results Phys*., **7** (2017), 1207−1211. https://doi.org/10.1016/j.rinp.2017.03.009
27. Y. M. Chu, N. Khan, M. I. Khan, K. Al-Khaled, N. Abbas, S. U. Khan, et al., Thermophoresis particle deposition analysis for nonlinear thermally developed flow of Magneto-Walter's B nanofluid with buoyancy forces, *Alex. Eng. J.*, **60** (2021), 1851−1860. https://doi.org/10.1016/j.aej.2020.11.033
28. F. Alzahrani, M. I. Khan, Significance of heat conduction in binary reactive flow of Walter's B fluid with radiative flux and activation energy, *Mod. Phys. Lett. B*, **35** (2021), 2140024. https://doi.org/10.1142/S0217984921400248
29. C. Ragavan, S. Munirathinam, M. Govindaraju, A. K. Abdul-Hakeem, B. Ganga, Elastic deformation and inclined magnetic field on entropy generation forwalter's liquid B fluid over a stretching sheet, *J. Appl. Math. Comput. Mech.*, **18** (2019). https://doi.org/10.17512/jamcm.2019.2.08
30. A. R. M. Kasim, *Free and mixed convective boundary layer flow of a viscoelastic fluid past a horizontal circular cylinder*, Universiti Teknologi Malaysia, 2011.
31. L. Ahmad, S. Javed, M. I. Khan, M. R. Khan, E. R. El-Zahar, A. A. A. Mousa, Non-axisymmetric Homann stagnation-point flow of unsteady Walter's B nanofluid over a vertical cylindrical disk, *P. I. Mech. Eng. E-J. Pro.*, 2021. https://doi.org/10.1177/09544089211064480
32. T. Hayat, Y. Wang, A. M. Siddiqui, K. Hutter, S. Asghar, Peristaltic transport of a third-order fluid in a circular cylindrical tube, *Math. Mod. Meth. Appl. S.*, **12** (2002), 1691−1706. https://doi.org/10.1142/S0218202502002288
33. B. J. Akinbo, Influence of convective boundary condition on heat and mass transfer in a Walters' B fluid over a vertical stretching surface with thermal-diffusion effect, *J. Therm. Eng.*, **7** (2021), 1784−1796. https://doi.org/10.18186/thermal.1026001
34. I. Khan, F. Ali, S. Shafie, M. Qasim, Unsteady free convection flow in a Walters-B fluid and heat transfer analysis, *B. Malays. Math. Sci. Soc.*, **37** (2014), 437−448.
35. D. Qaiser, Z. Zheng, M. R. Khan, Numerical assessment of mixed convection flow of Walters-B nanofluid over a stretching surface with Newtonian heating and mass transfer, *Therm. Sci. Eng. Prog.*, **22** (2021), 100801. https://doi.org/10.1016/j.tsep.2020.100801
36. K. Gangadhar, R. E. Nayak, M. V. S. Rao, T. Kannan, Nodal/Saddle stagnation point slip flow of an aqueous convectional magnesium oxide-gold hybrid nanofluid with viscous dissipation, *Arab. J. Sci. Eng.*, **46** (2021), 2701−2710. https://doi.org/10.1007/s13369-020-05195-x
37. K. Gangadhar, M. A. Kumari, A. J. Chamkha, EMHD flow of radiative second-grade nanofluid over a Riga Plate due to convective heating: Revised Buongiorno's nanofluid model, *Arab. J. Sci. Eng.*, **47** (2022), 8093−8103. https://doi.org/10.1007/s13369-021-06092-7
38. K. Gangadhar, M. A. Kumari, M. V. S. Rao, A. J. Chamkha, Oldroyd-B nanoliquid flow through a triple stratified medium submerged with gyrotactic bioconvection and nonlinear radiations, *Arab. J. Sci. Eng.*, **47** (2022), 8863–8875. https://doi.org/10.1007/s13369-021-06412-x

39. G. Kotha, V. R. Kolipaula, M. V. S. Rao, S. Penki, A. J. Chamkha, Internal heat generation on bioconvection of an MHD nanofluid flow due to gyrotactic microorganisms, *Eur. Phys. J. Plus*, **135** (2020), 1−19. https://doi.org/10.1140/epjp/s13360-020-00606-2
40. K. Gangadhar, K. B. Lakshmi, T. Kannan, A. J. Chamkha, Bioconvective magnetized oldroyd-B nanofluid flow in the presence of Joule heating with gyrotactic microorganisms, *Wave. Random Complex*, 2022, 1−21. https://doi.org/10.1080/17455030.2022.2050441
41. K. Gangadhar, A. J. Chamkha, Entropy minimization on magnetized Boussinesq couple stress fluid with non-uniform heat generation, *Phys. Scripta*, **96** (2021), 095205. https://doi.org/10.1088/1402-4896/ac03de
42. K. Gangadhar, K. B. Lakshmi, S. El-Sapa, M. V. S. Rao, A. J. Chamkha, Thermal energy transport of radioactive nanofluid flow submerged with microorganisms with zero mass flux condition, W*ave. Random Complex*, 2022, 1−23. https://doi.org/10.1080/17455030.2022.2072536
43. K. Gangadhar, E. M. Victoria, A. J. Chamkha, Hydrothermal features in the swirling flow of radiated graphene-Fe_3O_4 hybrid nanofluids through a rotating cylinder with exponential space-dependent heat generation, *Wave. Random Complex*, 2022, 1−24. https://doi.org/10.1080/17455030.2022.2100004
44. K. Gangadhar, M. Prameela, A. J. Chamkha, Exponential space-dependent heat generation on Powell-Eyring hybrid nanoliquid under nonlinear thermal radiation, *Indian J. Phys.*, **97** (2023), 2461–2473. https://doi.org/10.1007/s12648-022-02585-9
45. K. Gangadhar, P. M. Seshakumari, M. V. S. Rao, A. J. Chamkha, Biconvective transport of magnetized couple stress fluid over a radiative paraboloid of revolution, *P. I. Mech. Eng. E-J. Pro.*, **236** (2022), 1661−1670. https://doi.org/10.1177/09544089211072715
46. K. Gangadhar, R. E. Nayak, M. V. S. Rao, A. J. Chamkha, Nonlinear radiations in chemically reactive Walter's B nanoliquid flow through a rotating cone, *P. I. Mech. Eng. E-J. Pro.*, **237** (2023), 731−739. https://doi.org/10.1177/09544089221105932
47. D. N. Bhargavi, K. Gangadhar, A. J. Chamkha, Graphene-gold/PDMS Maxwell hybrid nanofluidic flow in a squeezed channel with linear and irregular radiations, *P. I. Mech. Eng. E-J. Pro.*, 2022. https://doi.org/10.1177/09544089221139696
48. H. Hanif, W. Jamshed, M. R. Eid, S. Shafie, R. W. Ibrahim, N. A. A. M. Nasir, et al., Thermal description and entropy evaluation of magnetized hybrid nanofluid with variable viscosity via Crank-Nicolson method, *Case Stud. Therm. Eng.*, **47** (2023), 103132. https://doi.org/10.1016/j.csite.2023.103132
49. H. Hanif, W. Jamshed, M. R. Eid, R. W. Ibrahim, S. Shafie, A. A. Raezah, et al., Numerical Crank-Nicolson methodology analysis for hybridity aluminium alloy nanofluid flowing based-water via stretchable horizontal plate with thermal resistive effect, *Case Stud. Therm. Eng.*, **42** (2023), 102707. https://doi.org/10.1016/j.csite.2023.102707
50. M. D. Shamshuddin, A. Saeed, S. R. Mishra, R. Katta, M. R. Eid, Homotopic simulation of MHD bioconvective flow of water-based hybrid nanofluid over a thermal convective exponential stretching surface, *Int. J. Numer. Method. H.*, **34** (2024), 31−53. https://doi.org/10.1108/HFF-03-2023-0128
51. Y. Li, M. Imtiaz, W. Jamshed, S. Rehman, M. R. Eid, N. A. A. M. Nasir, et al., Nonlinear thermal radiation and the slip effect on a 3D bioconvection flow of the Casson nanofluid in a rotating frame via a homotopy analysis mechanism, *Nanotechnol. Rev.*, **12** (2023), 20230161. https://doi.org/10.1515/ntrev-2023-0161
52. I. Ullah, W. A. Khan, W. Jamshed, A. Abd-Elmonem, N. S. E. Abdalla, R. W. Ibrahim, et al., Heat generation (absorption) in 3D bioconvection flow of Casson nanofluid via a convective heated stretchable surface, *J. Mol. Liq.*, **392** (2023), 123503. https://doi.org/10.1016/j.molliq.2023.123503

53. J. Bouslimi, A. A. Alkathiri, T. M. Althagafi, W. Jamshed, M. R. Eid, Thermal properties, flow and comparison between Cu and Ag nanoparticles suspended in sodium alginate as Sutterby nanofluids in solar collector, *Case Stud. Therm. Eng.*, **39** (2022), 102358. https://doi.org/10.1016/j.csite.2022.102358
54. A. D. Aldabesh, I. Tlili, Thermal enhancement and bioconvective analysis due to chemical reactive flow viscoelastic nanomaterial with modified heat theories: Bio-fuels cell applications, *Case Stud. Therm. Eng.*, **52** (2023), 103768. https://doi.org/10.1016/j.csite.2023.103768
55. Q. H. Le, K. Smida, Z. Abdelmalek, I. Tlili, Removal of heavy metals by polymers from wastewater in the industry: A molecular dynamics approach, *Eng. Anal. Bound. Elem.*, **155** (2023), 1035−1042. https://doi.org/10.1016/j.enganabound.2023.07.034
56. R. Sajjad, M. Hussain, S. U. Khan, A. Rehman, M. J. Khan, I. Tlili, et al., CFD analysis for different nanofluids in fin prolonged heat exchanger for waste heat recovery, *South Afr. J. Chem. Eng.*, **47** (2024), 9−14. https://doi.org/10.1016/j.sajce.2023.10.005
57. Z. Hussain, Z. U. Rehman, T. Abbas, K. Smida, Q. H. Le, Z. Abdelmalek, et al., Analysis of bifurcation and chaos in the traveling wave solution in optical fibers using the Radhakrishnan-Kundu-Lakshmanan equation, *Results Phys.*, **55** (2023), 107145. https://doi.org/10.1016/j.rinp.2023.107145
58. M. M. Bhatti, O. A. Bég, S. Kuharat, Electromagnetohydrodynamic (EMHD) convective transport of a reactive dissipative carreau fluid with thermal ignition in a non-Darcian vertical duct, *Numer. Heat Tr. A-Appl.*, 2023, 1−31. https://doi.org/10.1080/10407782.2023.2284333
59. M. M. Bhatti, S. Jun, C. M. Khalique, A. Shahid, L. Fasheng, M. S. Mohamed, Lie group analysis and robust computational approach to examine mass transport process using Jeffrey fluid model, *Appl. Math. Comput.*, **421** (2022), 126936. https://doi.org/10.1016/j.amc.2022.126936
60. K. Smida, M. U. Sohail, I. Tlili, A. Javed, Numerical thermal study of ternary nanofluid influenced by thermal radiation towards convectively heated sinusoidal cylinder, *Heliyon*, **9** (2023). https://doi.org/10.1016/j.heliyon.2023.e20057
61. I. Tlili, T. A. Alkanhal, A. Rebey, M. B. Henda, A. Sa'ed, Nanofluid bioconvective transport for non-Newtonian material in bidirectional oscillating regime with nonlinear radiation and external heat source: Applications to storage and renewable energy, *J. Energy Storage*, **68** (2023), 107839. https://doi.org/10.1016/j.est.2023.107839
62. C. Li, I. Tlili, Novel study of perovskite materials and the use of biomaterials to further solar cell application in the built environment: A molecular dynamic study, *Eng. Anal. Bound. Elem.*, **155** (2023), 425−431. https://doi.org/10.1016/j.enganabound.2023.06.018
63. Q. H. Le, F. Neila, K. Smida, Z. Li, Z. Abdelmalek, I. Tlili, pH-responsive anticancer drug delivery systems: Insights into the enhanced adsorption and release of DOX drugs using graphene oxide as a nanocarrier, *Eng. Anal. Bound. Elem.*, **157** (2023), 157−165. https://doi.org/10.1016/j.enganabound.2023.09.008
64. A. Abd-Elmonem, S. Kanwal, M. Imtiaz, K. Ali, S. Ahmad, W. Jamshed, et al., Case study of heat generation/absorption and activation energy on MHD hybrid nanofluid (GO-MoS_2/water) flow owing to a rotatfing disk, *Case Stud. Therm. Eng.*, **51** (2023), 103632. https://doi.org/10.1016/j.csite.2023.103632
65. M. R. Eid, W. Jamshed, A. Abd-Elmonem, A. F. Al-Hossainy, N. Almutlaq, A. Amjad, et al., Energy bandgap and thermal characteristics of non-Darcian MHD rotating hybridity nanofluid thin film flow: Nanotechnology application, *Nanotechnol. Rev.*, **12** (2023), 20230159. https://doi.org/10.1515/ntrev-2023-0159

66. N. Ullah, S. Nadeem, A. U. Khan, R. U. Haq, I. Tlili, Influence of metallic nanoparticles in water driven along a wavy circular cylinder, *Chinese J. Phys.*, **63** (2020), 168−185. https://doi.org/10.1016/j.cjph.2019.11.012
67. Z. Raizah, A. Saeed, M. Bilal, A. M. Galal, E. Bonyah, Parametric simulation of stagnation points flows of motile microorganism hybrid nanofluid across a circular cylinder with sinusoidal radius, *Open Phys.*, **21** (2023), 20220205. https://doi.org/10.1515/phys-2022-0205
68. M. Gholinia, K. Hosseinzadeh, D. D. Ganji, Investigation of different base fluids suspend by CNTs hybrid nanoparticle over a vertical circular cylinder with sinusoidal radius, *Case Stud. Therm. Eng.*, **21** (2020), 100666. https://doi.org/10.1016/j.csite.2020.100666
69. S. Dinarvand, R. Hosseini, E. Damangir, I. Pop, Series solutions for steady three-dimensional stagnation point flow of a nanofluid past a circular cylinder with sinusoidal radius variation, *Meccanica*, **48** (2013), 643−652. https://doi.org/10.1007/s11012-012-9621-7
70. P. Sunthrayuth, A. Alderremy, S. Aly, R. Shah, A. Akgül, Exact analysis of electro-osmotic flow of Walters'-B fluid with non-singular kernel, *Pramana*, **95** (2021), 1−10. https://doi.org/10.1007/s12043-021-02224-8
71. U. O. Mehmood, N. Mustapha, S. Shafie, Nonlinear peristaltic flow of Walter's B fluid in an asymmetric channel with heat transfer and chemical reactions, *Therm. Sci.*, **18** (2014), 1095−1107. https://doi.org/10.2298/TSCI110921096M
72. M. Arif, P. Kumam, W. Kumam, I. Khan, M. Ramzan, A fractional model of Casson fluid with ramped wall temperature: engineering applications of engine oil, *Comput. Math. Method.*, **3** (2021), e1162. https://doi.org/10.1002/cmm4.1162
73. M. H. Esfe, F. Zabihi, H. Rostamian, S. Esfandeh, Experimental investigation and model development of the non-Newtonian behavior of CuO-MWCNT-10w40 hybrid nano-lubricant for lubrication purposes, *J. Mol. Liq.*, **249** (2018), 677−687. https://doi.org/10.1016/j.molliq.2017.11.020
74. T. Sajid, A. A. Gari, W. Jamshed, M. R. Eid, N. Islam, K. Irshad, et al., Case study of autocatalysis reactions on tetra hybrid binary nanofluid flow via Riga wedge: Biofuel thermal application, *Case Stud. Therm. Eng.*, **47** (2023), 103058. https://doi.org/10.1016/j.csite.2023.103058
75. Z. A. Qureshi, S. Bilal, I. A. Shah, A. Akgül, R. Jarrar, H. Shanak, et al., Computational analysis of the morphological aspects of triadic hybridized magnetic nanoparticles suspended in liquid streamed in coaxially swirled disks, *Nanomaterials*, **12** (2022), 671. https://doi.org/10.3390/nano12040671
76. A. Hussain, M. Arshad, A. Hassan, A. Rehman, H. Ahmad, J. Baili, et al., Heat transport investigation of engine oil based rotating nanomaterial liquid flow in the existence of partial slip effect, *Case Stud. Therm. Eng.*, **28** (2021), 101500. https://doi.org/10.1016/j.csite.2021.101500
77. F. A. Soomro, R. U. Haq, M. Hamid, Brownian motion and thermophoretic effects on non-Newtonian nanofluid flow via Crank-Nicolson scheme, *Arch. Appl. Mech.*, **91** (2021), 3303−3313. https://doi.org/10.1007/s00419-021-01966-6
78. M. Ghani, Y. Norasia, I. Anggriani, M. Tafrikan, Z. Zulaikha, Numerical results of Crank-Nicolson scheme on unsteady nano fluid under the effect of Prandtl, Mixed Convection, and Magnetohydrodynamics, *Int. J. Comput. Sci. Appl. Math.*, **8** (2022), 71−78. https://doi.org/10.12962/j24775401.v8i2.14155
79. F. Waseem, M. Sohail, N. Ilyas, E. M. Awwad, M. Sharaf, M. J. Khan, et al., Entropy analysis of MHD hybrid nanoparticles with OHAM considering viscous dissipation and thermal radiation, *Sci. Rep.*, **14** (2024), 1096. https://doi.org/10.1038/s41598-023-50865-z
80. F. Wang, J. Zhang, S. Algarni, M. N. Khan, T. Alqahtani, S. Ahmad, Numerical simulation of hybrid Casson nanofluid flow by the influence of magnetic dipole and gyrotactic microorganism, *Wave. Random Complex*, 2022, 1−16. https://doi.org/10.1080/17455030.2022.2032866

81. F. Wang, M. Awais, R. Parveen, M. K. Alam, S. Rehman, N. A. Shah, Melting rheology of three-dimensional Maxwell nanofluid (Graphene-Engine-Oil) flow with slip condition past a stretching surface through Darcy-Forchheimer medium, *Results Phys.*, **51** (2023), 106647. https://doi.org/10.1016/j.rinp.2023.106647
82. S. Li, M. Sohail, U. Nazir, E. Sherif, A. Hassan, Statistical investigations and morphological aspects of cross-rheological material suspended in transportation of alumina, silica, titanium, and ethylene glycol via the Galerkin algorithm, *Nanotechnol. Rev.*, **12** (2023), 20230169. https://doi.org/10.1515/ntrev-2023-0169
83. F. Wang, Z. Iqbal, J. Zhang, M. A. Abdelmohimen, A. H. Almaliki, A. M. Galal, Bidirectional stretching features on the flow and heat transport of Burgers nanofluid subject to modified heat and mass fluxes, *Wave. Random Complex*, 2022, 1−18. https://doi.org/10.1080/17455030.2022.2055203

AIMS Press